

# On high-order pressure-robust space discretisations, their advantages for incompressible high Reynolds number generalised Beltrami flows and beyond

Nicolas R. Gauger<sup>a</sup>, Alexander Linke<sup>b,1,\*</sup>, Philipp W. Schroeder<sup>c,2</sup>

<sup>a</sup>*Chair for Scientific Computing, TU Kaiserslautern, 67663 Kaiserslautern, Germany*

<sup>b</sup>*Weierstrass Institute, 10117 Berlin, Germany*

<sup>c</sup>*Institute for Numerical and Applied Mathematics, Georg-August-Universität Göttingen, 37083 Göttingen, Germany*

## Abstract

Recently, high-order space discretisations were proposed for the numerical simulation of the incompressible Navier–Stokes equations at high Reynolds numbers, even for complicated domains from simulation practice. Although the overall spatial approximation order of the algorithms depends on the approximation quality of the boundary (often not better than third order), competitively accurate and efficient results were reported. In this contribution, first, a possible explanation for this somewhat surprising result is proposed: the velocity error of high-order space discretisations is more robust against quantitatively large and complicated pressure fields than low-order methods. Second, it is demonstrated that novel pressure-robust methods are significantly more accurate than comparable classical, non-pressure-robust space discretisations, whenever the quadratic, nonlinear convection term is a nontrivial gradient field like in certain generalised Beltrami flows at high Reynolds number. Then, pressure-robust methods even allow to halve the (formal) approximation order without compromising the accuracy. Third, classical high-order space discretisations are outperformed by pressure-robust methods whenever the boundary is not approximated with high-order accuracy. This improved accuracy of (low-order) pressure-robust mixed methods is explained in terms of a Helmholtz–Hodge projector, which cancels out the nonlinear convection term in any generalised Beltrami flow, since it is a gradient field. The numerical results are illustrated by a novel numerical analysis for pressure-robust and classical space discretisations. Further, the relevance of these results is discussed for flows that are not of Beltrami type.

*Keywords:* incompressible Navier–Stokes equations, pressure-robust methods, Helmholtz–Hodge projector, Discontinuous Galerkin method, divergence-free  $H(\text{div})$  finite elements, structure-preserving algorithms, high-order methods, (generalised) Beltrami flows, high Reynolds number flows

## 1 Introduction

In recent years high-order space discretisation was proposed as an efficient means for the simulation of challenging flow problems, like incompressible Navier–Stokes flows at high Reynolds numbers or real-world applications in computational fluid dynamics [54, 35]. The potential benefits of high-order discretisations are suggested to be twofold [54]:

- exponential convergence under certain regularity assumptions which can be achieved from a clever combination of high-quality mesh generation with  $p$ -refinement away from domain boundaries;

\*Corresponding author

*Email addresses:* nicolas.gauger@scicomp.uni-kl.de (Nicolas R. Gauger), alexander.linke@wias-berlin.de (Alexander Linke), p.schroeder@math.uni-goettingen.de (Philipp W. Schroeder)

<sup>1</sup>ORCID: <https://orcid.org/0000-0002-0165-2698>

<sup>2</sup>ORCID: <https://orcid.org/0000-0001-7644-4693>

- better diffusion and dispersion properties of the spatially discretised differential operators.

There are certainly potential benefits of smart  $h/p$ -refinement strategies. However, this contribution wants to discuss possible pitfalls and misinterpretations which could lead to overly optimistic conclusions concerning current high-order simulation results:

- while the approximation property argument of  $h/p$  methods is convincing, there is an inherent prerequisite in the argument: the availability of high-order boundary approximations of 3D mesh generators [54], since the approximation accuracy of the boundary restricts the maximally achievable approximation order of the entire algorithm. Put differently: if such a high quality mesh does not exist for a given complicated domain (as it often happens in practice; e.g. boundaries generated by CAD tools yield spline surfaces of third order), high-order methods will simply not achieve high-order convergence rates, as will be also illustrated below in this article; Then, possible advantages must have a different reason than the  $h/p$  approximation property argument.
- hidden consistency errors in state-of-the-art simulation codes which are reduced by higher-order methods, since such consistency errors are practically reduced by the simple mechanism of classical (high-order) Taylor expansion. In fact, the present contribution is only pointing to one hidden consistency error in nearly all computational fluid dynamics (CFD) space discretisations, which is related to some discrete Helmholtz–Hodge projector, resp., to some discrete curl operator therein [34].

In the context of the transient incompressible Navier–Stokes equations

$$\begin{cases} \partial_t \mathbf{u} - \nu \Delta \mathbf{u} + (\mathbf{u} \cdot \nabla) \mathbf{u} + \nabla p = \mathbf{f}, & (1a) \\ \nabla \cdot \mathbf{u} = 0, & (1b) \end{cases}$$

with constant kinematic viscosity  $\nu > 0$ , such a consistency error was recently identified as a lack of pressure-robustness [34, 39, 42]. Nearly all classical mixed methods like the Taylor–Hood element or (only  $L^2$ -conforming) Discontinuous Galerkin (DG) methods suffer from it. This means that the discrete velocity errors can become large whenever large gradient fields (and thus large pressure gradients) dominate the Navier–Stokes momentum balance. Please note that the nonlinear dynamics of the incompressible Navier–Stokes equations is completely driven by its vorticity equation

$$\omega_t - \nu \Delta \omega + (\mathbf{u} \cdot \nabla) \omega = \nabla \times \mathbf{f} + (\omega \cdot \nabla) \mathbf{u}, \quad (2)$$

which is formally derived from (1) by applying the curl operator to the momentum balance and substituting  $\omega := \nabla \times \mathbf{u}$ . Due to  $\nabla \times \nabla \phi = \mathbf{0}$ , the two forces  $\mathbf{f}$  and  $\mathbf{f} + \nabla \phi$  induce the same velocity field  $\mathbf{u}$ , independent of the scalar potential  $\phi$ . This leads to an equivalence class of forces, where two forces are equivalent if they differ only by an arbitrary gradient field, i.e.,

$$\mathbf{f} \simeq \mathbf{f} + \nabla \phi. \quad (3)$$

Note that this purely formal argument is made precise by introducing the Helmholtz–Hodge projector, which will be done below. The lack of pressure-robustness of classical methods is thus a consequence of a space discretisation which does not take into account the existence of such equivalence classes of forces. However, this consistency error of classical space discretisations is reduced dramatically by high-order methods (please note that a similar discussion of high-order methods versus well-balanced/structure-preserving methods is ongoing also in the hyperbolic conservation law community [30]). Especially, this can be observed in a specific, very rich physical regime, the so-called *generalised Beltrami flows*, where it holds  $(\mathbf{u} \cdot \nabla) \mathbf{u} \simeq \mathbf{0}$ , since  $(\mathbf{u} \cdot \nabla) \mathbf{u}$  itself equals a gradient field  $\nabla \phi$ . Generalised Beltrami flow comprise, e.g., all steady and time-dependent potential flows.

Conversely, it will be demonstrated that novel pressure-robust space discretisations, which are designed for an appropriate handling of the mentioned equivalence class of forces, sometimes even allow to halve the (formal)

approximation order of the applied algorithms (compared to classical methods) without compromising the accuracy. This holds when the flow is a high Reynolds number generalised Beltrami flow, which, in general, has a highly complicated pressure field. The maybe astonishing order reduction factor 2, which can be gained by pressure-robust mixed methods, is explained by the fact that in Beltrami flows the quadratic nonlinear convection term is balanced by the pressure gradient, i.e.,

$$(\mathbf{u} \cdot \nabla)\mathbf{u} = \frac{1}{2}\nabla|\mathbf{u}|^2 = \nabla p, \quad (4)$$

which leads to a complicated pressure term. Indeed, imagine the velocity field  $\mathbf{u}$  is a polynomial of order  $k$ , then the pressure  $p$  is a polynomial of order  $2k$ . A pressure-robust method of order  $k$  will deliver the exact velocity solution on every mesh, while classical, non-pressure-robust methods require a discrete pressure space of order  $2k$  in order to deliver the exact velocity field. This simple argument will be strengthened by a comparative numerical analysis of classical and pressure-robust space discretisations for time-dependent generalised Beltrami flows. The analysis exploits essentially the following three observations [1, 40]:

1. a pressure-robust space discretisation of the time-dependent Stokes equation for *small viscosities* is essentially error-free on finite (sufficiently short w.r.t. the viscosity) time-intervals, i.e., the approximation error of the initial values does not grow in time;
2. under the same conditions, classical space discretisations of the time-dependent Stokes problem do only suffer from large gradient fields in the momentum balance (large pressures), and discrete velocity errors induced by gradient fields accumulate over time;
3. for generalised Beltrami flows where the nonlinear term is balanced by the pressure gradient, the time evolution of the discrete Stokes equations (with a complicated pressure gradient) is a reasonable bound for the behaviour of the velocity error.

From a functional analysis point of view, the superior behaviour of pressure-robust space discretisations is explained by a corresponding more consistent discrete Helmholtz–Hodge projector. Note that for the infinite-dimensional Helmholtz–Hodge projector  $\mathbb{P}$  below, for all gradient fields with scalar potential  $\phi$ , there holds

$$\mathbb{P}(\nabla\phi) \equiv \mathbf{0}, \quad (5)$$

i.e., two forces  $\mathbf{f}$  and  $\mathbf{g}$  belong to the same equivalence class of forces if their Helmholtz–Hodge projectors coincide, namely

$$\mathbf{f} \simeq \mathbf{g} \quad \Leftrightarrow \quad \mathbb{P}(\mathbf{f}) = \mathbb{P}(\mathbf{g}). \quad (6)$$

While for the discrete Helmholtz–Hodge projector of pressure-robust methods likewise holds

$$\text{pressure-robust:} \quad \mathbb{P}_h(\nabla\phi) \equiv \mathbf{0}, \quad (7)$$

classical space discretisations possess corresponding discrete Helmholtz–Hodge projectors which have the consistency error

$$\text{classical mixed methods:} \quad \|\mathbb{P}_h(\nabla\phi)\|_{\mathbf{H}_h^{-1}(\Omega)} \lesssim h^{k_p+1} \|\phi\|_{H^{k_p+1}(\Omega)}, \quad (8)$$

where  $d \in \{2, 3\}$  defines the space dimension,  $h$  corresponds to the mesh size  $k_p$  denotes the (formal) approximation order of the discrete pressure space with respect to the (scalar)  $L^2$  norm [40, 39], and  $\mathbf{H}_h^{-1}(\Omega)$  denotes a discrete  $\mathbf{H}^{-1}(\Omega)$  norm. Moreover, if in a time-dependent setting with a fixed time interval  $[0, T]$  ( $T > 0$ ), the consistency error of  $\mathbb{P}_h(\nabla\phi)$  is estimated in the stronger  $L^2$  norm, then classical, non-pressure-robust methods lose further consistency by one order [42].

Indeed, the influence of the pressure  $p$ , which balances all gradient fields in the Navier–Stokes momentum balance, on the excitation of errors in the discrete velocities of classical mixed methods is essential. This issue has been a rather hot research topic in the beginning of the history of finite element methods for CFD [45, 23, 53, 29, 19, 27] — sometimes called *poor mass conservation* — and continued to be investigated for

many years [25, 48, 26, 50], often in connection with the so-called *grad-div stabilisation* [24, 44, 15, 32, 3]. However, it was understood better only recently that exactly the relaxation of the divergence constraint, which was invented in classical mixed methods in order to construct discretely inf-sup stable discretisation schemes, introduces the consistency error mentioned above. Consequently, *poor mass conservation* can be better described as a *poor momentum balance* [34, 38, 37] or a poor discretisation of a discrete curl operator, more precisely a poor discretisation of the Helmholtz–Hodge projector [40].

In the last part of this contribution, in order to demonstrate that the results for generalised Beltrami flows also matter to a certain degree for flow problems which do not strictly belong to this class of flows, a laminar Kármán vortex street at moderate Reynolds number is investigated numerically. More precisely, even though a particular flow might not be of generalised Beltrami type everywhere in the domain, the solution can indeed behave like one locally. This indicates an advantage of pressure-robust methods even for practically relevant flows which cannot be categorised as generalised Beltrami *per se*.

*Organisation of the article:* As a basis for this work, Section 2 introduces the flow regime of generalised Beltrami flows as a special class of incompressible flow solutions. Afterwards, in Section 3 the time-dependent Navier–Stokes problem, its weak formulation, the Helmholtz–Hodge projector and its discrete counterpart are discussed in an  $\mathbf{H}^1$ -conforming finite element setting. Also for  $\mathbf{H}^1$ -conforming FEM, a novel time-dependent  $\mathbf{L}^2$  *a priori* error analysis is presented in Section 4. It assumes a certain smoothness of the Navier–Stokes solution  $(\mathbf{u}, p)$ , leading to uniqueness, and it lays down the foundation for the main argument in Section 5 that pressure-robust space discretisations allow to reduce the approximation order on pre-asymptotic meshes without compromising the accuracy. Moving to computationally much more versatile  $\mathbf{L}^2$ - and  $\mathbf{H}(\text{div})$ -DG methods, Section 6 describes their space discretisation and the corresponding DG Helmholtz projectors. The remainder of the work is dedicated to numerical experiments: while Section 7 deals with generalised Beltrami flows with exact solutions in 2D and 3D, in Section 8 we go beyond this and show that locally, even practically more relevant flows can behave like a generalised Beltrami flow. Finally, some conclusions are drawn and an outlook is given in Section 9.

## 2 Generalised Beltrami flows

In this section, the reader is reminded that large velocity solution (sub-)sets of the time-dependent incompressible Navier–Stokes equations fulfil not only the Navier–Stokes equations but simultaneously the time-dependent Stokes equations, the time-dependent Euler equations and/or the PDE  $\partial_t \mathbf{u} + \nabla \pi = \mathbf{f}$ ,  $\nabla \cdot \mathbf{u} = 0$ . While the velocity solution remains the same, the pressure will change, though. Apart from the fact that this observation is clearly important for the construction of so-called *exact solutions* of the Navier–Stokes equations — i.e., solutions in the case  $\mathbf{f} = \mathbf{0}$  with an analytic expression for  $(\mathbf{u}, p)$  — and approximate solutions in the sense of asymptotic analysis, in this contribution we will exploit it in order to understand better how (space) discretisation errors develop in time-dependent simulations of the incompressible Navier–Stokes equations. Moreover, we will emphasise the impact of the continuous pressure  $p$  on the development of velocity errors.

Numerous velocity solutions  $\mathbf{u}$  of the transient incompressible Navier–Stokes equations (1) are actually velocity solutions of the transient, incompressible Stokes equations

$$\begin{cases} \partial_t \mathbf{u} - \nu \Delta \mathbf{u} + \nabla \pi = \mathbf{f}, & (9a) \\ \nabla \cdot \mathbf{u} = 0, & (9b) \end{cases}$$

where only the Stokes pressure  $\pi$  is different from the Navier–Stokes pressure  $p$ . For the practically important case with  $\mathbf{f} = \mathbf{0}$ , these velocity solutions build an entire class, and form a very rich subset of velocity solutions, which are classically called *generalised Beltrami flows*. The main observation for the understanding of this

class is the following pointwise identity for the nonlinear convection term:

$$(\mathbf{u} \cdot \nabla) \mathbf{u} = (\nabla \times \mathbf{u}) \times \mathbf{u} + \frac{1}{2} \nabla |\mathbf{u}|^2 = \boldsymbol{\omega} \times \mathbf{u} + \frac{1}{2} \nabla |\mathbf{u}|^2, \quad (10)$$

where  $\boldsymbol{\omega} \times \mathbf{u}$  is usually called the *Lamb vector*. Then, generalised Beltrami flows can be subdivided into three different subclasses:

1. The most famous generalised Beltrami flows are classical potential flows with  $\mathbf{u} = \nabla h$ , where  $h$  denotes a (possibly time-dependent) harmonic potential fulfilling  $-\Delta h = 0$ . Since potential flows are irrotational, it holds  $\boldsymbol{\omega} = \nabla \times \mathbf{u} = \nabla \times (\nabla h) = \mathbf{0}$  and the nonlinear convection term is a gradient field

$$(\mathbf{u} \cdot \nabla) \mathbf{u} = \frac{1}{2} \nabla |\mathbf{u}|^2, \quad (11)$$

and the nonlinear convection term is balanced by a pressure gradient  $\nabla p = -\frac{1}{2} \nabla |\mathbf{u}|^2$ . Thus,  $\mathbf{u}$  simultaneously fulfils the incompressible Navier–Stokes (1) and the incompressible Stokes equations (9). However, the Navier–Stokes and the Stokes pressure gradients differ and it holds

$$\nabla \pi = \nabla p + \frac{1}{2} \nabla |\mathbf{u}|^2 = \mathbf{0}. \quad (12)$$

Moreover, in addition to the Stokes and the Navier–Stokes equations, potential flows also fulfil the incompressible Euler equations since the friction term  $-\nu \Delta \mathbf{u} = -\nu \Delta (\nabla h) = -\nu \nabla (\Delta h) = \mathbf{0}$  vanishes everywhere, and the velocity time derivative  $\partial_t \mathbf{u} = \partial_t \nabla h = \nabla (\partial_t h)$  is a gradient field, which can be balanced by another contribution in the pressure gradient [39]. By the way, note that a time-dependent potential flow also fulfils the PDE  $\partial_t \mathbf{u} + \nabla \pi = \mathbf{0}$ ,  $\nabla \cdot \mathbf{u} = 0$ .

2. The second subclass consists of Beltrami flows. Contrary to potential flows, they are not irrotational, i.e., it holds  $\boldsymbol{\omega} \neq \mathbf{0}$ , however it holds  $\boldsymbol{\omega} \times \mathbf{u} = \mathbf{0}$ , i.e., the vorticity vector of Beltrami flows is parallel to the velocity field. Beltrami flows fulfil the incompressible Stokes equations (with the same pressure  $\pi = p + \frac{1}{2} |\mathbf{u}|^2 + \text{const}$  like in potential flows) and the Navier–Stokes equations, but usually not the incompressible Euler equations. They are sensible only in the three-dimensional case, because the vorticity of two-dimensional flows is always perpendicular to the velocity field.
3. Finally, for generalised Beltrami flows the vorticity is neither zero, nor is it parallel to the flow field, and even though the Lamb vector does not vanish in general, it is a gradient field with

$$\boldsymbol{\omega} \times \mathbf{u} = \nabla \phi. \quad (13)$$

Then  $\mathbf{u}$  fulfils the incompressible Stokes equations with the pressure gradient  $\nabla \pi = \nabla (p + \frac{1}{2} |\mathbf{u}|^2 + \phi)$ .

Overall, it should be emphasised that the vorticity equation of all generalised Beltrami flows is linear and given by

$$\partial_t \boldsymbol{\omega} - \nu \Delta \boldsymbol{\omega} = \mathbf{0}. \quad (14)$$

In some sense, it is this linearity which makes generalised Beltrami flows, even at high Reynolds numbers, computable; at least if pressure-robust space discretisations are used [50].

### 3 Time-dependent Navier–Stokes problem and $H^1$ discretisation

After a very brief introduction to the governing equations on the continuous level, we introduce the spatial  $H^1$ -conforming discretisation schemes which will be used for the error analysis in the first part of this work. They consist of an exactly divergence-free, pressure-robust method and a classical non-pressure-robust FEM.

### 3.1 Infinite-dimensional Navier–Stokes equations

We consider the time-dependent incompressible Navier–Stokes problem, which reads

$$\begin{cases} \partial_t \mathbf{u} - \nu \Delta \mathbf{u} + (\mathbf{u} \cdot \nabla) \mathbf{u} + \nabla p = \mathbf{f} & \text{in } (0, T] \times \Omega, \\ \nabla \cdot \mathbf{u} = 0 & \text{in } (0, T] \times \Omega, \\ \mathbf{u}(0, \mathbf{x}) = \mathbf{u}_0(\mathbf{x}) & \text{for } \mathbf{x} \in \Omega. \end{cases} \quad (15a)$$

$$\quad (15b)$$

$$\quad (15c)$$

For the space dimension  $d \in \{2, 3\}$ ,  $\Omega \subset \mathbb{R}^d$  denotes a connected bounded Lipschitz domain and  $T$  is the end of time considered in the particular problem. Since in the numerical analysis below we want to compare the best possible convergence rates for pressure-robust and classical space discretisations in the  $\mathbf{L}^2$ -norm, we will assume for technical reasons that  $\Omega$  is convex, leading to elliptic regularity. Moreover,  $\mathbf{u}: [0, T] \times \Omega \rightarrow \mathbb{R}^d$  indicates the velocity field,  $p: [0, T] \times \Omega \rightarrow \mathbb{R}$  is the (zero-mean) kinematic pressure,  $\mathbf{f}: [0, T] \times \Omega \rightarrow \mathbb{R}^d$  represents external body forces and  $\mathbf{u}_0: \Omega \rightarrow \mathbb{R}^d$  stands for a suitable initial condition for the velocity. The underlying fluid is assumed to be Newtonian with constant (dimensionless) kinematic viscosity  $0 < \nu \ll 1$ . We impose either the general Dirichlet boundary condition  $\mathbf{u} = \mathbf{g}_D$  on  $(0, T] \times \partial\Omega$ , or periodic boundary conditions (or a mixture of them).

*Notation:* In what follows, for  $K \subseteq \Omega$  we use the standard Sobolev spaces  $W^{m,p}(K)$  for scalar-valued functions with associated norms  $\|\cdot\|_{W^{m,p}(K)}$  and seminorms  $|\cdot|_{W^{m,p}(K)}$  for  $m \geq 0$  and  $p \geq 1$ . We obtain the Lebesgue space  $W^{0,p}(K) = L^p(K)$  and the Hilbert space  $W^{m,2}(K) = H^m(K)$ . Additionally, the closed subspaces  $H_0^1(K)$  consisting of  $H^1(K)$ -functions with vanishing trace on  $\partial K$  and the set  $L_0^2(K)$  of  $L^2(K)$ -functions with zero mean in  $K$  play an important role. The  $L^2(K)$ -inner product is denoted by  $(\cdot, \cdot)_K$  and, if  $K = \Omega$ , we sometimes omit the domain completely when no confusion can arise. Furthermore, with regard to time-dependent problems, given a Banach space  $\mathbf{X}$  and a time instance  $t$ , the Bochner space  $L^p(0, t; \mathbf{X})$  for  $p \in [1, \infty]$  is used. In the case  $t = T$ , we frequently use the abbreviation  $L^p(\mathbf{X}) = L^p(0, T; \mathbf{X})$ . Further,  $C^1(0, t; \mathbf{X})$  denotes the function space mapping  $[0, t]$  into  $\mathbf{X}$ , which is continuously differentiable in time w.r.t. the norm  $\|\mathbf{u}\|_{C^1(0,t;\mathbf{X})} = \max_{s \in [0,T]} (\|\mathbf{u}\|_{\mathbf{X}} + \|\mathbf{u}_t\|_{\mathbf{X}})$ . Spaces and norms for vector- and tensor-valued functions are indicated with bold letters. For example, for a vector-valued function  $\mathbf{v} = (v_1, \dots, v_n)^\dagger$ , we consider  $\|\mathbf{v}\|_{\mathbf{L}^p(\Omega)}^p = \sum_{i=1}^n \|v_i\|_{L^p(\Omega)}^p = \int_{\Omega} |\mathbf{v}|_p^p \, d\mathbf{x}$ , where  $|\mathbf{v}|_p^p = \sum_{i=1}^n |v_i|^p$ .

Depending on the particular boundary conditions, let  $\mathbf{V}/Q$  be the continuous solution spaces for velocity and pressure, respectively. Note that it holds  $\mathbf{V} \subset \mathbf{H}^1(\Omega)$  and  $Q \subset L^2(\Omega)$ . For the numerical analysis in this and the next section, we will always choose  $\mathbf{V} = \mathbf{H}_0^1(\Omega)$  and  $Q_h = L_0^2(\Omega)$ . The subspace of weakly divergence-free functions is defined as

$$\mathbf{V}^{\text{div}} = \{\mathbf{v} \in \mathbf{V} : (q, \nabla \cdot \mathbf{v}) = 0, \forall q \in Q\}.$$

A weak velocity solution  $\mathbf{u} \in L^2(0, T; \mathbf{V}^{\text{div}})$  of (15) fulfils that for all test functions  $\mathbf{v} \in \mathbf{V}^{\text{div}}$  holds

$$\frac{d}{dt} (\mathbf{u}(t), \mathbf{v}) + \nu (\nabla \mathbf{u}(t), \nabla \mathbf{v}) + ((\mathbf{u}(t) \cdot \nabla) \mathbf{u}(t), \mathbf{v}) = (\mathbf{f}(t), \mathbf{v})_{\mathbf{H}^{-1}, \mathbf{H}_0^1} \quad (16)$$

in the sense of distributions in  $\mathcal{D}'(]0, T[)$  and such that  $\mathbf{u}(0) = \mathbf{u}_0$  [12]. Note that the pressure  $p$  is not part of the weak formulation of the incompressible Navier–Stokes problem, see Remark 3.6. For the numerical analysis, we will further assume the regularities  $\mathbf{u} \in C^1(0, T; \mathbf{W}^{1,\infty}) \cap L^2(0, T; \mathbf{H}^2)$  and  $p \in L^\infty(0, T; H^1)$ , assuring, e.g., uniqueness of the weak solution in time [8, 51]. Then,  $(\mathbf{u}, p)$  fulfils

$$\begin{cases} \text{Find } (\mathbf{u}, p): (0, T] \rightarrow \mathbf{V} \times Q \text{ with } \mathbf{u}(0) = \mathbf{u}_0 \text{ s.t., } \forall (\mathbf{v}, q) \in \mathbf{V} \times Q, \\ (\partial_t \mathbf{u}, \mathbf{v}) + \nu (\nabla \mathbf{u}, \nabla \mathbf{v}) + ((\mathbf{u} \cdot \nabla) \mathbf{u}, \mathbf{v}) - (p, \nabla \cdot \mathbf{v}) + (q, \nabla \cdot \mathbf{u}) = (\mathbf{f}, \mathbf{v}). \end{cases} \quad (17a)$$

$$\quad (17b)$$

### 3.2 Helmholtz–Hodge decomposition in $L^2$

In order to understand the significance of pressure-robustness for the discretisation theory of the incompressible Navier–Stokes equations (15), the concept of the Helmholtz–Hodge projector is introduced. Since the numerical analysis below is essentially an  $L^2$  analysis (assuming all forces  $\partial_t \mathbf{u}(t)$ ,  $(\mathbf{u}(t) \cdot \nabla) \mathbf{u}(t)$ , ... to be in  $L^2$ ), we will restrict our considerations to the Helmholtz–Hodge decomposition in  $L^2$ . Below in this section, some functional analytic prerequisites are summarised that show that only the divergence-free parts, i.e., the Helmholtz–Hodge projectors of the forces in the Navier–Stokes momentum balance influence the velocity solution of the incompressible Navier–Stokes equations, see also [34].

The space of square-integrable divergence-free (solenoidal) vector fields is defined by

$$\mathbf{L}_\sigma^2(\Omega) := \{ \mathbf{w} \in \mathbf{L}^2(\Omega) : -(\mathbf{w}, \nabla \phi) = 0, \forall \phi \in H^1(\Omega) \}. \quad (18)$$

**REMARK 3.1:** First note that for  $\phi \in C_0^\infty(\Omega)$  the mapping  $\phi \mapsto -(\mathbf{w}, \nabla \phi)$  denotes the distributional divergence of  $\mathbf{w}$ . Thus, vector fields in  $\mathbf{L}_\sigma^2(\Omega)$  are divergence-free [34]. Further note that definition (18) implies that  $\mathbf{w} \cdot \mathbf{n}|_{\partial\Omega} = 0$ , where  $\mathbf{n}$  denotes the outer unit normal vector on  $\partial\Omega$ , since test functions  $\phi \in H^1$  do not vanish on the boundary of  $\Omega$ . In this context, please also note that a Helmholtz–Hodge decomposition is made unique only by prescribing certain boundary conditions. The reason is that any gradient of a harmonic function with  $-\Delta h = 0$  is irrotational and divergence-free at the same time. Thus, the boundary conditions determine whether  $\nabla h$  is called ‘divergence-free’ or ‘gradient field’. In our setting, all gradients of harmonic functions are called ‘gradient fields’, and vector fields in  $\mathbf{L}_\sigma^2(\Omega)$  are orthogonal to all gradient fields in  $L^2$ .

**REMARK 3.2:** Our considerations regard the Helmholtz–Hodge decomposition in  $L^2$  of  $(\mathbf{u} \cdot \nabla) \mathbf{u}$ . Since we assume that  $\mathbf{u} \in \mathbf{W}^{1,\infty}$ , it holds  $(\mathbf{u} \cdot \nabla) \mathbf{u} \in L^2$ .

Due to the special choice of the boundary conditions and Remark 3.1 one obtains:

#### THEOREM 3.3 (Helmholtz–Hodge decomposition in $L^2$ )

For every vector field  $\mathbf{v} \in \mathbf{L}^2(\Omega)$ , there exists a unique Helmholtz–Hodge decomposition

$$\mathbf{v} = \mathbf{w} + \nabla \psi, \quad (19)$$

where it holds  $\mathbf{w} \in \mathbf{L}_\sigma^2(\Omega)$ , and  $\psi \in H^1(\Omega)$  and  $\mathbf{w}$  and  $\nabla \psi$  are  $L^2$ -orthogonal. Then,  $\mathbf{w} =: \mathbb{P}(\mathbf{v})$  is called the Helmholtz–Hodge projector of  $\mathbf{v}$ .

**PROOF:** A potential  $\psi \in H^1(\Omega)/\mathbb{R}$  in the Helmholtz–Hodge decomposition is obtained by: for all  $\chi \in H^1(\Omega)/\mathbb{R}$  holds

$$(\nabla \psi, \nabla \chi) = (\mathbf{v}, \nabla \chi). \quad (20)$$

This Neumann problem for  $\psi$  is uniquely solvable [34]. Then, define  $\mathbf{w} := \mathbf{v} - \nabla \psi$ . One can test  $\mathbf{w}$  with arbitrary gradient fields  $\nabla(\phi + C)$ , where  $C$  denotes an arbitrary real number and where it holds  $\phi \in H^1(\Omega)/\mathbb{R}$ . Then, one obtains  $(\mathbf{w}, \nabla(\phi + C)) = (\mathbf{w}, \nabla \phi) = (\mathbf{v} - \nabla \psi, \nabla \phi) = 0$ , due to (20). Thus, it holds  $\mathbf{w} \in \mathbf{L}_\sigma^2(\Omega)$ . Due to the definition of  $\mathbf{L}_\sigma^2(\Omega)$ ,  $\mathbf{w}$  and  $\nabla \psi$  are orthogonal in  $L^2$ . Assuming that  $\mathbf{v} = \mathbf{w}_1 + \nabla \psi_1 = \mathbf{w}_2 + \nabla \psi_2$  are two Helmholtz–Hodge decompositions of  $\mathbf{v}$ , then it holds

$$\mathbf{w}_1 - \mathbf{w}_2 = \nabla(\psi_2 - \psi_1)$$

with  $\mathbf{w}_1 - \mathbf{w}_2 \in \mathbf{L}_\sigma^2(\Omega)$ . Testing this equality by  $\nabla(\psi_1 - \psi_2)$  yields by the  $L^2$ -orthogonality of (20)

$$\|\nabla(\psi_2 - \psi_1)\|_{L^2(\Omega)}^2 = 0,$$

and one concludes  $\mathbf{w}_1 = \mathbf{w}_2$  and  $\psi_1 = \psi_2$  using  $\psi_1, \psi_2 \in H^1(\Omega)/\mathbb{R}$ . Thus, the Helmholtz–Hodge decomposition is unique. ■

**REMARK 3.4:** Formally, the Helmholtz–Hodge decomposition of  $\mathbf{v} \in \mathbf{L}^2(\Omega)$  can be written as the solution of the PDE problem

$$\begin{cases} \mathbb{P}(\mathbf{v}) + \nabla\psi = \mathbf{v} & \text{in } \Omega, \\ \nabla \cdot \mathbb{P}(\mathbf{v}) = 0 & \text{in } \Omega, \\ \mathbb{P}(\mathbf{v}) \cdot \mathbf{n} = 0 & \text{on } \partial\Omega. \end{cases} \quad \begin{array}{l} (21a) \\ (21b) \\ (21c) \end{array}$$

The most important property of the Helmholtz–Hodge projector for our contribution is given by:

**LEMMA 3.5**

For all  $\psi \in H^1(\Omega)$ , it holds

$$\mathbb{P}(\nabla\psi) = \mathbf{0}.$$

**PROOF:** Note that  $\nabla\psi = \mathbf{0} + \nabla\psi$  is the unique Helmholtz–Hodge decomposition of  $\nabla\psi$ . Thus, it follows  $\mathbb{P}(\nabla\psi) = \mathbf{0}$ .  $\blacksquare$

Finally, it is emphasised that the velocity solution  $\mathbf{u}$  of (16) is completely determined by testing the momentum equation with divergence-free velocity test functions  $\mathbf{v} \in \mathbf{V}^{\text{div}}$  and by its initial value  $\mathbf{u}_0$ . Assuming smoothness of  $\mathbf{u}$  in space and time,  $\mathbf{u}$  fulfils for all  $\mathbf{v} \in \mathbf{V}^{\text{div}}$

$$(\partial_t \mathbf{u}, \mathbf{v}) + \nu(\nabla \mathbf{u}, \nabla \mathbf{v}) + ((\mathbf{u} \cdot \nabla) \mathbf{u}, \mathbf{v}) = (\mathbf{f}, \mathbf{v}) \quad \Leftrightarrow \quad (22a)$$

$$(\mathbb{P}(\partial_t \mathbf{u}), \mathbf{v}) - \nu(\mathbb{P}(\Delta \mathbf{u}), \mathbf{v}) + (\mathbb{P}((\mathbf{u} \cdot \nabla) \mathbf{u}), \mathbf{v}) = (\mathbb{P}(\mathbf{f}), \mathbf{v}). \quad (22b)$$

**REMARK 3.6:** Equation (22a) shows that the velocity solution  $\mathbf{u}$  of the incompressible Navier–Stokes equations is not determined by the forces  $\mathbf{f}$  in the momentum equation themselves, but by their Helmholtz–Hodge projectors  $\mathbb{P}(\mathbf{f})$ . Therefore, two forces  $\mathbf{f}$  and  $\mathbf{g}$  that differ by a gradient field  $\mathbf{f} = \mathbf{g} + \nabla\phi$ , lead to the same velocity solution. Thus, the velocity solution of the incompressible Navier–Stokes equations is naturally determined by equivalence classes of forces, where it holds

$$\mathbf{f} \simeq \mathbf{g} \quad \Leftrightarrow \quad \mathbb{P}(\mathbf{f}) = \mathbb{P}(\mathbf{g}).$$

### 3.3 $H^1$ finite element methods

Let  $\mathbf{V}_h/Q_h$  be the considered discretely inf-sup stable velocity/pressure FE pair, where  $\mathbf{V}_h \subset \mathbf{V}$  and  $Q_h \subset Q$ . We assume that the discrete velocity space contains polynomials up to degree  $k_u$  and the discrete pressure space contains polynomials up to degree  $k_p$ . Note that for most discretely inf-sup stable schemes it holds  $k_p = k_u - 1$ . An example is the Taylor–Hood finite element family  $\mathbf{P}_k/\mathbb{P}_{k-1}$  with  $k \geq 2$  [33]. However, for the famous mini element it holds  $k_p = k_u (= 1)$  [6]. In the following numerical analysis,  $C > 0$  always denotes a generic constant, whose value is independent of the mesh size but possibly dependent on the mesh-regularity.

In order to approximate (15), or equivalently (17), the following generic semi-discrete FEM is considered:

$$\left\{ \begin{array}{l} \text{Find } (\mathbf{u}_h, p_h): (0, T] \rightarrow \mathbf{V}_h \times Q_h \text{ with } \mathbf{u}_h(0) = \mathbf{u}_{0h} \text{ s.t., } \forall (\mathbf{v}_h, q_h) \in \mathbf{V}_h \times Q_h, \\ (\partial_t \mathbf{u}_h, \mathbf{v}_h) + \nu(\nabla \mathbf{u}_h, \nabla \mathbf{v}_h) + \left( (\mathbf{u}_h \cdot \nabla) \mathbf{u}_h + \frac{1}{2}(\nabla \cdot \mathbf{u}_h) \mathbf{u}_h, \mathbf{v}_h \right) - (p_h, \nabla \cdot \mathbf{v}_h) + (q_h, \nabla \cdot \mathbf{u}_h) = (\mathbf{f}, \mathbf{v}_h). \end{array} \right.$$

Now, the choice of the FE spaces decides whether an exactly divergence-free, pressure-robust method is applied or not. For example, the Scott–Vogelius element  $\mathbf{P}_k/\mathbb{P}_{k-1}^{\text{dc}}$  is discretely inf-sup stable on shape-regular, barycentrically refined meshes for  $k \geq d$  [57]; then it yields an exactly divergence-free and thus pressure-robust method. On the other hand, for example, a classical Taylor–Hood element is a non-pressure-robust method. Note that the explicit skew-symmetrisation of the convective term is only necessary for a non-divergence-free FEM.



The subspace of discretely divergence-free functions is given by

$$\mathbf{V}_h^{\text{div}} = \{\mathbf{v}_h \in \mathbf{V}_h : (q_h, \nabla \cdot \mathbf{v}_h) = 0, \forall q_h \in Q_h\},$$

where we note that for exactly divergence-free (and thus pressure-robust) FEM,  $\mathbf{v}_h \in \mathbf{V}_h^{\text{div}}$  follows  $\nabla \cdot \mathbf{v}_h = 0$ , i.e.,  $\mathbf{V}_h^{\text{div}} \subset \mathbf{L}_\sigma^2(\Omega)$ . In this context, a frequently used tool in finite element error analysis is the discrete Stokes projector, defined by

$$\mathbb{S}_h : \mathbf{V}^{\text{div}} \rightarrow \mathbf{V}_h^{\text{div}}, \quad \mathbb{S}_h(\mathbf{v}) = \arg \min_{\mathbf{v}_h \in \mathbf{V}_h^{\text{div}}} \|\nabla(\mathbf{v} - \mathbf{v}_h)\|_{\mathbf{L}^2(\Omega)}, \quad \int_{\Omega} \nabla[\mathbb{S}(\mathbf{v}) - \mathbf{v}] : \nabla \mathbf{v}_h \, d\mathbf{x} = 0, \quad \forall \mathbf{v}_h \in \mathbf{V}_h^{\text{div}}.$$

The Stokes projector possesses optimal approximation properties due to discrete inf-sup stability [1]. Last but not least, the Lagrange interpolation into the  $H^1$ -conforming subspace of the discrete pressure-space  $Q_h$  is denoted by

$$L_h : C(\bar{\Omega}) \rightarrow Q_h \cap H^1(\Omega). \quad (24)$$

**REMARK 3.7:** For discrete discontinuous pressure spaces with  $k_p \geq 1$  it holds for all  $q \in H^{k_p+1}$

$$\|\nabla(q - L_h q)\|_{\mathbf{L}^2} \leq Ch^{k_p} |q|_{H^{k_p+1}(\Omega)},$$

where  $C$  does only depend on the shape-regularity of the triangulation.

**LEMMA 3.8 (Convergence of the nonlinear convection term as  $h \rightarrow 0$ )**

Assume that  $\mathbf{u}_h \rightarrow \mathbf{u} \in \mathbf{W}^{1,\infty}(\Omega)$  converges strongly in  $\mathbf{H}^1(\Omega)$  and that  $\|\mathbf{u}_h\|_{\mathbf{W}^{1,\infty}(\Omega)} \leq C$  is uniformly bounded. Then,  $(\mathbf{u}_h \cdot \nabla)\mathbf{u}_h \rightarrow (\mathbf{u} \cdot \nabla)\mathbf{u}$  converges strongly in  $\mathbf{L}^2(\Omega)$ . Further, it holds that  $\mathbb{P}((\mathbf{u}_h \cdot \nabla)\mathbf{u}_h) \rightarrow \mathbb{P}((\mathbf{u} \cdot \nabla)\mathbf{u})$  converges strongly for the Helmholtz–Hodge projector in  $\mathbf{L}^2(\Omega)$ .

**PROOF:** One can derive

$$\begin{aligned} \|(\mathbf{u}_h \cdot \nabla)\mathbf{u}_h - (\mathbf{u} \cdot \nabla)\mathbf{u}\|_{\mathbf{L}^2(\Omega)} &\leq \|((\mathbf{u}_h - \mathbf{u}) \cdot \nabla)\mathbf{u}_h\|_{\mathbf{L}^2(\Omega)} + \|(\mathbf{u} \cdot \nabla)(\mathbf{u}_h - \mathbf{u})\|_{\mathbf{L}^2(\Omega)} \\ &\leq \|\mathbf{u}_h - \mathbf{u}\|_{\mathbf{L}^2(\Omega)} \|\nabla \mathbf{u}_h\|_{\mathbf{L}^\infty(\Omega)} + \|\mathbf{u}\|_{\mathbf{L}^\infty(\Omega)} \|\nabla(\mathbf{u}_h - \mathbf{u})\|_{\mathbf{L}^2(\Omega)}. \end{aligned}$$

Due to  $\mathbf{u}_h \rightarrow \mathbf{u}$  strongly in  $\mathbf{H}^1(\Omega)$ ,  $\|\mathbf{u}_h - \mathbf{u}\|_{\mathbf{L}^2(\Omega)}$  and  $\|\nabla(\mathbf{u}_h - \mathbf{u})\|_{\mathbf{L}^2(\Omega)}$  converge to zero. Further,  $\|\nabla \mathbf{u}_h\|_{\mathbf{L}^\infty(\Omega)}$  and  $\|\mathbf{u}\|_{\mathbf{L}^\infty(\Omega)}$  are assumed to be bounded. The convergence of the Helmholtz–Hodge projectors  $\mathbb{P}((\mathbf{u}_h \cdot \nabla)\mathbf{u}_h) \rightarrow \mathbb{P}((\mathbf{u} \cdot \nabla)\mathbf{u})$  in  $\mathbf{L}^2(\Omega)$  is an immediate consequence of the well-posedness of the Neumann problem (20) in  $H^1(\Omega)/\mathbb{R}$ . ■

**REMARK 3.9:** When confronted with generalised Beltrami flows at high Reynolds numbers, Lemma 3.8 is decisive in order to understand the behaviour of space discretisations of the incompressible Navier–Stokes equations. While  $\mathbb{P}((\mathbf{u} \cdot \nabla)\mathbf{u})$  vanishes for generalised Beltrami flows since  $(\mathbf{u} \cdot \nabla)\mathbf{u}$  is a gradient field, on the discrete level  $\mathbb{P}((\mathbf{u}_h \cdot \nabla)\mathbf{u}_h) \rightarrow \mathbf{0}$  holds since  $(\mathbf{u}_h \cdot \nabla)\mathbf{u}_h$  only converges to a gradient field as  $h \rightarrow 0$ . Thus, one can observe some kind of *pseudo-dominant* convection at high Reynolds numbers [39], i.e., the infinite-dimensional generalised Beltrami problem is not convection-dominated due to  $\mathbb{P}((\mathbf{u} \cdot \nabla)\mathbf{u}) = \mathbf{0}$ , but the discretised problem experiences some non-negligible, artificial convective force. A similar effect can be observed also for the linear Stokes problem when one uses numerical quadratures in the discretisation of forces of gradient fields, see [41, Subsection 6.2].

### 3.4 Discrete $H^1$ -conforming Helmholtz–Hodge projector

A discrete Helmholtz–Hodge projector in  $\mathbf{L}^2$  is defined straightforward as the  $\mathbf{L}^2$  projector onto  $\mathbf{V}_h^{\text{div}}$ :

$$\mathbb{P}_h : \mathbf{L}^2(\Omega) \rightarrow \mathbf{V}_h^{\text{div}}, \quad \mathbb{P}_h(\mathbf{v}) = \arg \min_{\mathbf{v}_h \in \mathbf{V}_h^{\text{div}}} \|\mathbf{v} - \mathbf{v}_h\|_{\mathbf{L}^2(\Omega)}, \quad \int_{\Omega} [\mathbb{P}_h(\mathbf{v}) - \mathbf{v}] \cdot \mathbf{v}_h \, d\mathbf{x} = 0, \quad \forall \mathbf{v}_h \in \mathbf{V}_h^{\text{div}}. \quad (25)$$

**REMARK 3.10:** Under the assumptions of elliptic regularity of  $\Omega$ , shape-regular meshes and discrete inf-sup stability of the method, the corresponding discrete Helmholtz projector has optimal approximation properties

$$\|\mathbf{u} - \mathbb{P}_h(\mathbf{u})\|_{\mathbf{L}^2(\Omega)} + h \|\nabla[\mathbf{u} - \mathbb{P}_h(\mathbf{u})]\|_{\mathbf{L}^2(\Omega)} \leq Ch^{k+1} \|\mathbf{u}\|_{\mathbf{H}^{k+1}(\Omega)}. \quad (26)$$

The proof follows directly from [1, Lemma 11].

**LEMMA 3.11** ( *$\mathbf{W}^{1,\infty}$  stability of discrete Helmholtz–Hodge projector*)

Assume elliptic regularity of  $\Omega$ , shape-regular meshes, discrete inf-sup stability of the method and that the exact solution  $\mathbf{u}$  is sufficiently smooth. Then, the corresponding discrete Helmholtz–Hodge projector fulfils

$$\|\nabla \mathbb{P}_h(\mathbf{u})\|_{\mathbf{L}^\infty(\Omega)} \leq C \|\nabla \mathbf{u}\|_{\mathbf{L}^\infty(\Omega)} + h^{k_u - d/2} \|\mathbf{u}\|_{\mathbf{H}^{k+1}(\Omega)}, \quad (27)$$

where  $C > 0$  is independent of  $h$  and  $k_u$  denotes the polynomial order of discrete velocities in  $\mathbf{V}_h$ .

**PROOF:** The first step is to use the Stokes projector and the triangle inequality to obtain

$$\|\nabla \mathbb{P}_h(\mathbf{u})\|_{\mathbf{L}^\infty(\Omega)} \leq \|\nabla \mathbb{S}_h(\mathbf{u})\|_{\mathbf{L}^\infty(\Omega)} + \|\nabla \mathbb{P}_h(\mathbf{u}) - \nabla \mathbb{S}_h(\mathbf{u})\|_{\mathbf{L}^\infty(\Omega)}.$$

Note that the  $\mathbf{W}^{1,\infty}$  stability of the Stokes projector has been shown in [28]. For shape-regular decompositions  $\mathcal{T}_h$ , the discrete space  $\mathbf{V}_h$  (and thus also  $\mathbf{V}_h^{\text{div}}$ ) satisfies the local inverse inequality [21, Lemma 1.138]

$$\forall \mathbf{v}_h \in \mathbf{V}_h: \quad \|\mathbf{v}_h\|_{\mathbf{W}^{\ell,p}(K)} \leq C_{\text{inv}} h_K^{m-\ell+d(\frac{1}{p}-\frac{1}{q})} \|\mathbf{v}_h\|_{\mathbf{W}^{m,q}(K)}, \quad \forall K \in \mathcal{T}_h, \quad (28)$$

where  $0 \leq m \leq \ell$  and  $1 \leq p, q \leq \infty$ . Choosing  $\ell = m = 1$ ,  $p = \infty$  and  $q = 2$ , the inverse estimate can be applied to further estimate the right-hand side as

$$\begin{aligned} \|\nabla \mathbb{P}_h(\mathbf{u}) - \nabla \mathbb{S}_h(\mathbf{u})\|_{\mathbf{L}^\infty(\Omega)} &\leq C_{\text{inv}} h^{-d/2} \|\nabla[\mathbb{P}_h(\mathbf{u}) - \mathbb{S}_h(\mathbf{u})]\|_{\mathbf{L}^2(\Omega)} \\ &\leq C_{\text{inv}} h^{-d/2} \left[ \|\nabla[\mathbf{u} - \mathbb{P}_h(\mathbf{u})]\|_{\mathbf{L}^2(\Omega)} + \|\nabla[\mathbf{u} - \mathbb{S}_h(\mathbf{u})]\|_{\mathbf{L}^2(\Omega)} \right] \\ &\leq Ch^{k_u - d/2} \|\mathbf{u}\|_{\mathbf{H}^{k_u+1}(\Omega)}, \end{aligned}$$

where the optimal approximation properties of both  $\mathbb{P}_h$  and  $\mathbb{S}_h$  are essential. ■

Combining Lemmas 3.11 and 3.8 yields a result which is essential for good convergence properties of the Galerkin method on pre-asymptotic meshes, see also Theorems 4.1 and 4.5:

**REMARK 3.12:** Assuming  $k_u \geq d/2$ , it holds for  $h \rightarrow 0$  that

$$\mathbb{P}((\mathbb{P}_h(\mathbf{u}) \cdot \nabla) \mathbb{P}_h(\mathbf{u})) \xrightarrow{\mathbf{L}^2} \mathbb{P}((\mathbf{u} \cdot \nabla) \mathbf{u}).$$

Now, let us first consider the situation where  $\mathbb{P}_h$  belongs to a pressure-robust (divergence-free) method.

**LEMMA 3.13**

For pressure-robust (divergence-free)  $\mathbf{H}^1$  methods, for all  $\psi \in H^1(\Omega)$  it holds

$$\mathbb{P}_h(\nabla \psi) = \mathbf{0}.$$

**PROOF:** Since for divergence-free methods  $\nabla \cdot \mathbf{v}_h = 0$  holds for all  $\mathbf{v}_h \in \mathbf{V}_h^{\text{div}}$ , one obtains

$$(\nabla \psi, \mathbf{v}_h) = -(\psi, \nabla \cdot \mathbf{v}_h) = 0,$$

for all  $\mathbf{v}_h \in \mathbf{V}_h^{\text{div}}$ . ■

Finally, for non-pressure-robust methods, the situation is not exactly the same as in the infinite-dimensional case. In fact, for the steady Navier–Stokes problem, i.e., for the elliptic problem, one has to estimate the consistency error of  $\mathbb{P}_h(\nabla\phi)$  in a discrete  $\mathbf{H}_h^{-1}$  norm, which yields an  $\mathcal{O}(h^{k_p+1})$  consistency error [40], where  $k_p$  denotes the formal approximation order of the discrete pressure space in the  $L^2$  norm. However, for the fully time-dependent *a priori* error analysis below we will have to estimate this consistency error in the stronger  $\mathbf{L}^2(\Omega)$  norm, which was seemingly done for the first time in [42].

**LEMMA 3.14**

For non-pressure-robust  $\mathbf{H}^1$  methods with  $k_p \geq 1$ , it holds for all gradient fields  $\nabla\psi$  with  $\psi \in H^{k_p+1}(\Omega)$

$$\|\mathbb{P}_h(\nabla\psi)\|_{\mathbf{L}^2(\Omega)} \leq Ch^{k_p} |\psi|_{H^{k_p+1}(\Omega)}. \quad (29)$$

**PROOF:** Given  $\psi \in H^{k_p+1}(\Omega)$ , it holds for all discretely divergence-free  $\mathbf{v}_h \in \mathbf{V}_h^{\text{div}}$

$$0 = -(L_h\psi, \nabla \cdot \mathbf{v}_h) = (\nabla(L_h\psi), \mathbf{v}_h),$$

due to  $L_h\psi \in Q_h \cap H^1(\Omega)$ . Thus, one obtains

$$(\nabla\psi, \mathbf{v}_h) = (\nabla(\psi - L_h\psi), \mathbf{v}_h) \leq \|\nabla(\psi - L_h\psi)\|_{\mathbf{L}^2(\Omega)} \|\mathbf{v}_h\|_{\mathbf{L}^2(\Omega)}.$$

The result is proven using Remark 3.7. ■

**REMARK 3.15:** The numerical experiments in [42] indicate that Lemma 3.14 is sharp. Indeed, for non-pressure-robust, inf-sup stable mixed methods with discontinuous  $\mathbb{P}_0$  pressures, i.e.,  $k_p = 0$ , like the nonconforming Crouzeix–Raviart and the conforming Bernardi–Raugel element, it is demonstrated that it holds

$$\|\mathbb{P}_h(\nabla q)\|_{\mathbf{L}^2(\Omega)} = \mathcal{O}(1),$$

leading to a pressure-induced locking phenomenon for the time-dependent Stokes equations in the presence of large pressure gradients.

**REMARK 3.16:** Remark 3.12 assures that at least for  $k_u \geq d/2$  one obtains for  $h \rightarrow 0$  the convergence result

$$\mathbb{P}((\mathbb{P}_h(\mathbf{u}) \cdot \nabla)\mathbb{P}_h(\mathbf{u})) \xrightarrow{\mathbf{L}^2} \mathbb{P}((\mathbf{u} \cdot \nabla)\mathbf{u}).$$

However, the quality of the space discretisation (23) is determined by whether and how

$$\mathbb{P}_h((\mathbb{P}_h(\mathbf{u}) \cdot \nabla)\mathbb{P}_h(\mathbf{u})) \xrightarrow{\mathbf{L}^2} \mathbb{P}((\mathbf{u} \cdot \nabla)\mathbf{u})$$

converges for  $h \rightarrow 0$ . For  $k_p \geq 2$ , convergence in  $\mathbf{L}^2$  is assured. But the convergence speed of pressure-robust methods can be much faster than in classical, non-pressure-robust space discretisations due to Lemma 3.14, when  $(\mathbf{u} \cdot \nabla)\mathbf{u}$  contains a large gradient part in the sense of the Helmholtz–Hodge decomposition (19). This is the main reason for the superiority of pressure-robust methods for Beltrami flows, where space discretisations suffer from an artificial, pseudo-dominant convection on coarse meshes, see Remark 3.9. Exactly this artificial pseudo-dominant convection is reduced by pressure-robust methods.

## 4 A special $H^1$ finite element error analysis

In the following, we present a numerical error analysis for the time-dependent Navier–Stokes problem which is based on a new understanding of the velocity error in the time-dependent Stokes problem, see [42] and [1, Section 4]. The key point is that in the case of low viscosities, pressure-robust space discretisations do not show an increase in the velocity error as long as the time interval is small compared with  $\nu^{-1}$ . On

the other hand, in non-pressure-robust methods the only source of error is a dominating pressure gradient in the momentum balance [2, Theorem 5.2]; namely in the special case  $\mathbf{f} = \text{const}$  one gets (for  $\nu \ll 1$ )  $\mathbf{u}_h \approx \mathbb{P}_h(\mathbf{u}) + t\mathbb{P}_h(\nabla p)$  for  $t \in [0, T]$ .

In the following, we will give two different error estimates for the Navier–Stokes equations in the pressure-robust and the non-pressure-robust case. The convergence analysis is inspired by novel discrete velocity error estimates for the transient Stokes equations [42, 40, 1], which estimate the difference between the discrete velocity  $\mathbf{u}_h(t)$  and the (discretely divergence-free)  $L^2$  best approximation  $\mathbb{P}_h(\mathbf{u}(t))$ .

#### 4.1 Pressure-robust space discretisation

##### THEOREM 4.1 (Pressure-robust estimate)

For the discrete velocity for all  $t \in [0, T]$  the following representation is chosen

$$\mathbf{u}_h(t) = \mathbb{P}_h(\mathbf{u}(t)) + \mathbf{e}_h(t),$$

and the time-dependent evolution of  $\mathbf{e}_h(t)$  is considered. Then, on the time interval  $[0, T]$ ,  $\mathbf{e}_h$  can be estimated by

$$\begin{aligned} \|\mathbf{e}_h(T)\|_{L^2}^2 + \nu \|\nabla \mathbf{e}_h\|_{L^2(L^2)}^2 &\leq e^{1+2\|\nabla \mathbb{P}_h(\mathbf{u})\|_{L^1(L^\infty)}} \times \left( \nu \|\nabla [\mathbb{S}_h(\mathbf{u}) - \mathbb{P}_h(\mathbf{u})]\|_{L^2(L^2)}^2 \right. \\ &\quad \left. + 2T \int_0^T \|\nabla \mathbb{P}_h(\mathbf{u})\|_{L^\infty}^2 \|\mathbf{u} - \mathbb{P}_h(\mathbf{u})\|_{L^2}^2 + \|\mathbf{u}\|_{L^\infty}^2 \|\nabla [\mathbf{u} - \mathbb{P}_h(\mathbf{u})]\|_{L^2}^2 \, d\tau \right). \end{aligned}$$

**REMARK 4.2:** Due to the explicit  $2T$  dependence of the error in Theorem 4.1, in the case  $T \gg \nu^{-1}$  this estimate can become pessimistic. Note that for our numerical examples in Section 7, we indeed consider short time intervals for which Theorem 4.1 is meaningful. In the literature, usually one can find ‘long-term’ estimates, e.g., [9, 14, 5, 51, 50], which are sharper for  $T \gg \nu^{-1}$ , but which are pessimistic for short time intervals.

**PROOF OF THEOREM 4.1:** Note that  $\nabla \cdot \mathbf{z}_h = 0$  for all  $\mathbf{z}_h \in \mathbf{V}_h^{\text{div}}$  due to  $\mathbf{V}_h^{\text{div}} \subset \mathbf{L}_\sigma^2(\Omega)$  assuming pressure-robustness. Due to Galerkin orthogonality, for all  $\mathbf{z}_h \in \mathbf{V}_h^{\text{div}}$  it holds

$$\begin{aligned} (\partial_t \mathbf{u}_h, \mathbf{z}_h) + \nu(\nabla \mathbf{u}_h, \nabla \mathbf{z}_h) + ((\mathbf{u}_h \cdot \nabla) \mathbf{u}_h, \mathbf{z}_h) &= (\partial_t \mathbf{u}, \mathbf{z}_h) + \nu(\nabla \mathbf{u}, \nabla \mathbf{z}_h) + ((\mathbf{u} \cdot \nabla) \mathbf{u}, \mathbf{z}_h) \\ &= (\partial_t \mathbb{P}_h(\mathbf{u}), \mathbf{z}_h) + \nu(\nabla \mathbb{S}_h(\mathbf{u}), \nabla \mathbf{z}_h) + ((\mathbf{u} \cdot \nabla) \mathbf{u}, \mathbf{z}_h). \end{aligned}$$

Here, it was used  $(\nabla p, \mathbf{z}_h) = 0$ , which is equivalent to  $\mathbb{P}_h(\nabla p) = \mathbf{0}$ , proved in Lemma 3.13 for pressure-robust space discretisations. Using the representation  $\mathbf{u}_h(t) = \mathbb{P}_h(\mathbf{u}(t)) + \mathbf{e}_h(t)$  leads to: for all  $\mathbf{z}_h \in \mathbf{V}_h^{\text{div}}$  holds

$$(\partial_t \mathbf{e}_h, \mathbf{z}_h) + \nu(\nabla \mathbf{e}_h, \nabla \mathbf{z}_h) + (([\mathbb{P}_h(\mathbf{u}) + \mathbf{e}_h] \cdot \nabla) [\mathbb{P}_h(\mathbf{u}) + \mathbf{e}_h], \mathbf{z}_h) = \nu(\nabla (\mathbb{S}_h(\mathbf{u}) - \mathbb{P}_h(\mathbf{u})), \nabla \mathbf{z}_h) + ((\mathbf{u} \cdot \nabla) \mathbf{u}, \mathbf{z}_h),$$

where the initial value for the ODE system is chosen as  $\mathbf{e}_h(0) = \mathbf{0}$ . For the discrete nonlinear term, we obtain

$$\begin{aligned} (([\mathbb{P}_h(\mathbf{u}) + \mathbf{e}_h] \cdot \nabla) [\mathbb{P}_h(\mathbf{u}) + \mathbf{e}_h], \mathbf{z}_h) &= ((\mathbf{e}_h \cdot \nabla) \mathbf{e}_h, \mathbf{z}_h) + ((\mathbb{P}_h(\mathbf{u}) \cdot \nabla) \mathbf{e}_h, \mathbf{z}_h) \\ &\quad + ((\mathbf{e}_h \cdot \nabla) \mathbb{P}_h(\mathbf{u}), \mathbf{z}_h) + ((\mathbb{P}_h(\mathbf{u}) \cdot \nabla) \mathbb{P}_h(\mathbf{u}), \mathbf{z}_h). \end{aligned}$$

Further, due to the skew-symmetry of the first two terms plus  $\nabla \cdot \mathbf{e}_h = \nabla \cdot \mathbb{P}_h(\mathbf{u}) = 0$ , testing with  $\mathbf{z}_h = \mathbf{e}_h$  leads to

$$\begin{aligned} \frac{1}{2} \frac{d}{dt} \|\mathbf{e}_h\|_{L^2}^2 + \nu \|\nabla \mathbf{e}_h\|_{L^2}^2 \\ = \nu(\nabla [\mathbb{S}_h(\mathbf{u}) - \mathbb{P}_h(\mathbf{u})], \nabla \mathbf{e}_h) - ((\mathbf{e}_h \cdot \nabla) \mathbb{P}_h(\mathbf{u}), \mathbf{e}_h) - ((\mathbb{P}_h(\mathbf{u}) \cdot \nabla) \mathbb{P}_h(\mathbf{u}), \mathbf{e}_h) + ((\mathbf{u} \cdot \nabla) \mathbf{u}, \mathbf{e}_h). \end{aligned}$$

Due to Lemmas 3.8 and 3.11, the last two terms on the right-hand side can be combined and estimated by

$$\begin{aligned} & ((\mathbb{P}_h(\mathbf{u}) \cdot \nabla) \mathbb{P}_h(\mathbf{u}) - (\mathbf{u} \cdot \nabla) \mathbf{u}, \mathbf{e}_h) = (([\mathbb{P}_h(\mathbf{u}) - \mathbf{u}] \cdot \nabla) \mathbb{P}_h(\mathbf{u}) + (\mathbf{u} \cdot \nabla) [\mathbb{P}_h(\mathbf{u}) - \mathbf{u}], \mathbf{e}_h) \\ & \leq \|\nabla \mathbb{P}_h(\mathbf{u})\|_{\mathbf{L}^\infty} \|\mathbf{u} - \mathbb{P}_h(\mathbf{u})\|_{\mathbf{L}^2} \|\mathbf{e}_h\|_{\mathbf{L}^2} + \|\mathbf{u}\|_{\mathbf{L}^\infty} \|\nabla [\mathbf{u} - \mathbb{P}_h(\mathbf{u})]\|_{\mathbf{L}^2} \|\mathbf{e}_h\|_{\mathbf{L}^2} \\ & \leq T \left( \|\nabla \mathbb{P}_h(\mathbf{u})\|_{\mathbf{L}^\infty}^2 \|\mathbf{u} - \mathbb{P}_h(\mathbf{u})\|_{\mathbf{L}^2}^2 + \|\mathbf{u}\|_{\mathbf{L}^\infty}^2 \|\nabla [\mathbf{u} - \mathbb{P}_h(\mathbf{u})]\|_{\mathbf{L}^2}^2 \right) + \frac{1}{2T} \|\mathbf{e}_h\|_{\mathbf{L}^2}^2. \end{aligned}$$

Here, the weight  $(2T)^{-1}$  in front of  $\|\mathbf{e}_h\|_{\mathbf{L}^2}^2$  ensures that later on, the argument of the exponential Gronwall term does not catch any explicit  $T$  dependence. The other convection term can be treated simply by the generalised Hölder inequality; that is,

$$((\mathbf{e}_h \cdot \nabla) \mathbb{P}_h(\mathbf{u}), \mathbf{e}_h) \leq \|\nabla \mathbb{P}_h(\mathbf{u})\|_{\mathbf{L}^\infty} \|\mathbf{e}_h\|_{\mathbf{L}^2}^2.$$

Using Young's inequality for the remaining term involving Stokes and Helmholtz–Hodge projectors, after rearranging, one obtains the overall estimate

$$\begin{aligned} \frac{d}{dt} \|\mathbf{e}_h\|_{\mathbf{L}^2}^2 + \nu \|\nabla \mathbf{e}_h\|_{\mathbf{L}^2}^2 & \leq \nu \|\nabla [\mathbb{S}_h(\mathbf{u}) - \mathbb{P}_h(\mathbf{u})]\|_{\mathbf{L}^2}^2 + \left( \frac{1}{T} + 2 \|\nabla \mathbb{P}_h(\mathbf{u})\|_{\mathbf{L}^\infty} \right) \|\mathbf{e}_h\|_{\mathbf{L}^2}^2 \\ & \quad + 2T \left( \|\nabla \mathbb{P}_h(\mathbf{u})\|_{\mathbf{L}^\infty}^2 \|\mathbf{u} - \mathbb{P}_h(\mathbf{u})\|_{\mathbf{L}^2}^2 + \|\mathbf{u}\|_{\mathbf{L}^\infty}^2 \|\nabla [\mathbf{u} - \mathbb{P}_h(\mathbf{u})]\|_{\mathbf{L}^2}^2 \right). \end{aligned}$$

In such a situation, Gronwall's lemma [33, Lemma A.54] in differential form states that for  $t \in [0, T]$ ,

$$\frac{d}{dt} \|\mathbf{e}_h(t)\|_{\mathbf{L}^2}^2 \leq \alpha(t) + \beta(t) \|\mathbf{e}_h(t)\|_{\mathbf{L}^2}^2 \quad \Rightarrow \quad \|\mathbf{e}_h(t)\|_{\mathbf{L}^2}^2 \leq \int_0^t \alpha(s) \exp \left( \int_s^t \beta(\tau) d\tau \right) ds. \quad (30)$$

In order to apply this estimate, one sets

$$\beta(t) = \frac{1}{T} + 2 \|\nabla \mathbb{P}_h(\mathbf{u})\|_{\mathbf{L}^\infty}$$

and

$$\begin{aligned} \alpha(t) & = -\nu \|\nabla \mathbf{e}_h\|_{\mathbf{L}^2}^2 + \nu \|\nabla [\mathbb{S}_h(\mathbf{u}) - \mathbb{P}_h(\mathbf{u})]\|_{\mathbf{L}^2}^2 \\ & \quad + 2T \left( \|\nabla \mathbb{P}_h(\mathbf{u})\|_{\mathbf{L}^\infty}^2 \|\mathbf{u} - \mathbb{P}_h(\mathbf{u})\|_{\mathbf{L}^2}^2 + \|\mathbf{u}\|_{\mathbf{L}^\infty}^2 \|\nabla [\mathbf{u} - \mathbb{P}_h(\mathbf{u})]\|_{\mathbf{L}^2}^2 \right), \end{aligned}$$

and computes for  $t \geq s$

$$\exp \left( \int_s^t \beta(\tau) d\tau \right) = \exp \left( \frac{t-s}{T} + 2 \|\nabla \mathbb{P}_h(\mathbf{u})\|_{L^1(s,t;\mathbf{L}^\infty)} \right).$$

Using  $0 \leq s \leq t \leq T$  and  $0 \leq \frac{t-s}{T} \leq 1$ , one obtains

$$c \exp \left( \frac{t-s}{T} + 2 \|\nabla \mathbb{P}_h(\mathbf{u})\|_{L^1(s,t;\mathbf{L}^\infty)} \right) \leq \begin{cases} c \exp \left( 1 + 2 \|\nabla \mathbb{P}_h(\mathbf{u})\|_{L^1(\mathbf{L}^\infty)} \right) & \text{for } c \geq 0, \\ c & \text{for } c < 0. \end{cases}$$

Now, actually applying Gronwall's lemma yields the estimate

$$\begin{aligned} \|\mathbf{e}_h(T)\|_{\mathbf{L}^2}^2 & \leq \int_0^T \alpha(s) \exp \left( \int_s^T \beta(\tau) d\tau \right) ds \leq -\nu \|\nabla \mathbf{e}_h\|_{\mathbf{L}^2(\mathbf{L}^2)}^2 + e^{1+2\|\nabla \mathbb{P}_h(\mathbf{u})\|_{L^1(\mathbf{L}^\infty)}} \\ & \quad \times \left( \nu \|\nabla [\mathbb{S}_h(\mathbf{u}) - \mathbb{P}_h(\mathbf{u})]\|_{\mathbf{L}^2(\mathbf{L}^2)}^2 + 2T \int_0^T \|\nabla \mathbb{P}_h(\mathbf{u})\|_{\mathbf{L}^\infty}^2 \|\mathbf{u} - \mathbb{P}_h(\mathbf{u})\|_{\mathbf{L}^2}^2 + \|\mathbf{u}\|_{\mathbf{L}^\infty}^2 \|\nabla [\mathbf{u} - \mathbb{P}_h(\mathbf{u})]\|_{\mathbf{L}^2}^2 d\tau \right). \end{aligned}$$

Rearranging concludes the proof. ■

**REMARK 4.3:** The estimate in Theorem 4.1 is pressure-robust, since if  $\mathbf{u}(t) \in \mathbf{V}_h^{\text{div}}$  holds for all  $t \in [0, T]$ , then it also holds  $\mathbf{u}_h(t) = \mathbf{u}(t)$  due to  $\mathbf{u} = \mathbb{S}_h(\mathbf{u}) = \mathbb{P}_h(\mathbf{u})$ , i.e., the pressure  $p$  does not spoil the discrete velocity solution  $\mathbf{u}_h$ .

**REMARK 4.4:** Note that under the assumption that  $k_u$  is large enough and  $h$  is small enough, one can apply Lemma 3.11 to obtain  $\|\nabla \mathbb{P}_h(\mathbf{u})\|_{\mathbf{L}^\infty} \leq C \|\nabla \mathbf{u}\|_{\mathbf{L}^\infty}$ .

## 4.2 Classical space discretisation

### THEOREM 4.5 (Non-pressure-robust estimate)

For the discrete velocity for all  $t \in [0, T]$  the following representation is chosen

$$\mathbf{u}_h(t) = \mathbb{P}_h(\mathbf{u}(t)) + \mathbf{e}_h(t),$$

and the time-dependent evolution of  $\mathbf{e}_h(t)$  is considered. Then, on the time interval  $[0, T]$ ,  $\mathbf{e}_h$  can be estimated by

$$\begin{aligned} \|\mathbf{e}_h(T)\|_{\mathbf{L}^2}^2 + \nu \|\nabla \mathbf{e}_h\|_{\mathbf{L}^2(\mathbf{L}^2)}^2 &\leq e^{1+4\|\nabla \mathbb{P}_h(\mathbf{u})\|_{\mathbf{L}^1(\mathbf{L}^\infty)}} \times \left( \nu \|\nabla[\mathbb{S}_h(\mathbf{u}) - \mathbb{P}_h(\mathbf{u})]\|_{\mathbf{L}^2(\mathbf{L}^2)}^2 \right. \\ &\quad + 3T \|\nabla[p - L_h(p)]\|_{\mathbf{L}^2(\mathbf{L}^2)}^2 + 3T \int_0^T \left[ \|\mathbb{P}_h(\mathbf{u})\|_{\mathbf{L}^\infty}^2 \|\nabla \cdot \mathbb{P}_h(\mathbf{u})\|_{\mathbf{L}^2}^2 \right. \\ &\quad \left. \left. + 2 \|\nabla \mathbb{P}_h(\mathbf{u})\|_{\mathbf{L}^\infty}^2 \|\mathbf{u} - \mathbb{P}_h(\mathbf{u})\|_{\mathbf{L}^2}^2 + 2 \|\mathbf{u}\|_{\mathbf{L}^\infty}^2 \|\nabla[\mathbf{u} - \mathbb{P}_h(\mathbf{u})]\|_{\mathbf{L}^2}^2 \right] d\tau \right). \end{aligned}$$

**PROOF OF THEOREM 4.5:** Following the same procedure as for the pressure-robust case, one obtains

$$\begin{aligned} \frac{1}{2} \frac{d}{dt} \|\mathbf{e}_h\|_{\mathbf{L}^2}^2 + \nu \|\nabla \mathbf{e}_h\|_{\mathbf{L}^2}^2 &= \nu (\nabla[\mathbb{S}_h(\mathbf{u}) - \mathbb{P}_h(\mathbf{u})], \nabla \mathbf{e}_h) + (\nabla[p - L_h(p)], \mathbf{e}_h) + ((\mathbf{u} \cdot \nabla) \mathbf{u}, \mathbf{e}_h) \\ &\quad - \left( (\mathbf{e}_h \cdot \nabla) \mathbb{P}_h(\mathbf{u}) + \frac{1}{2} (\nabla \cdot \mathbf{e}_h) \mathbb{P}_h(\mathbf{u}), \mathbf{e}_h \right) - \left( (\mathbb{P}_h(\mathbf{u}) \cdot \nabla) \mathbb{P}_h(\mathbf{u}) + \frac{1}{2} (\nabla \cdot \mathbb{P}_h(\mathbf{u})) \mathbb{P}_h(\mathbf{u}), \mathbf{e}_h \right). \end{aligned}$$

Note that in the non-pressure-robust case the pressure contribution does not vanish, since it holds  $\mathbf{V}_h^{\text{div}} \not\subset \mathbf{L}_\sigma^2(\Omega)$  and the consistency error  $\|\mathbb{P}_h(\nabla p)\|_{\mathbf{L}^2(\Omega)}$  estimated in Lemma 3.14 unavoidably appears in the estimate. Further, the full skew-symmetric convective term has to be taken into account. In comparison to the pressure-robust case, there are only two new contributions from the skew-symmetrisation of the convective term which have to be estimated. For the first one,

$$\begin{aligned} \left( \frac{1}{2} (\nabla \cdot \mathbb{P}_h(\mathbf{u})) \mathbb{P}_h(\mathbf{u}), \mathbf{e}_h \right) &= \left( \frac{1}{2} (\nabla \cdot [\mathbf{u} - \mathbb{P}_h(\mathbf{u})]) \mathbb{P}_h(\mathbf{u}), \mathbf{e}_h \right) \leq \|\mathbb{P}_h(\mathbf{u})\|_{\mathbf{L}^\infty} \|\nabla \cdot [\mathbf{u} - \mathbb{P}_h(\mathbf{u})]\|_{\mathbf{L}^2} \|\mathbf{e}_h\|_{\mathbf{L}^2} \\ &\leq \frac{3T}{2} \|\mathbb{P}_h(\mathbf{u})\|_{\mathbf{L}^\infty}^2 \|\nabla \cdot [\mathbf{u} - \mathbb{P}_h(\mathbf{u})]\|_{\mathbf{L}^2}^2 + \frac{1}{6T} \|\mathbf{e}_h\|_{\mathbf{L}^2}^2 \end{aligned}$$

can be obtained. Applying Young's inequality slightly differently than in the pressure-robust case leads to

$$\begin{aligned} ((\mathbb{P}_h(\mathbf{u}) \cdot \nabla) \mathbb{P}_h(\mathbf{u}) - (\mathbf{u} \cdot \nabla) \mathbf{u}, \mathbf{e}_h) &\leq \frac{6T}{2} \left( \|\nabla \mathbb{P}_h(\mathbf{u})\|_{\mathbf{L}^\infty}^2 \|\mathbf{u} - \mathbb{P}_h(\mathbf{u})\|_{\mathbf{L}^2}^2 + \|\mathbf{u}\|_{\mathbf{L}^\infty}^2 \|\nabla[\mathbf{u} - \mathbb{P}_h(\mathbf{u})]\|_{\mathbf{L}^2}^2 \right) + \frac{1}{6T} \|\mathbf{e}_h\|_{\mathbf{L}^2}^2. \end{aligned}$$

With the help of integration by parts, the additional contribution in the remaining additional convective term can be estimated as

$$\left( \frac{1}{2} (\nabla \cdot \mathbf{e}_h) \mathbb{P}_h(\mathbf{u}), \mathbf{e}_h \right) = -\frac{1}{2} ((\nabla \mathbb{P}_h(\mathbf{u})) \mathbf{e}_h, \mathbf{e}_h) \leq \|\nabla \mathbb{P}_h(\mathbf{u})\|_{\mathbf{L}^\infty} \|\mathbf{e}_h\|_{\mathbf{L}^2}^2.$$

For completeness, from the pressure-robust case, we repeat

$$((\mathbf{e}_h \cdot \nabla) \mathbb{P}_h(\mathbf{u}), \mathbf{e}_h) \leq \|\nabla \mathbb{P}_h(\mathbf{u})\|_{\mathbf{L}^\infty} \|\mathbf{e}_h\|_{\mathbf{L}^2}^2.$$

Finally, the additional pressure term can be bounded as follows:

$$(\nabla[p - L_h(p)], \mathbf{e}_h) \leq \frac{3T}{2} \|\nabla[p - L_h(p)]\|_{\mathbf{L}^2}^2 + \frac{1}{6T} \|\mathbf{e}_h\|_{\mathbf{L}^2}^2$$

This yields the overall estimate

$$\begin{aligned} & \frac{d}{dt} \|\mathbf{e}_h\|_{\mathbf{L}^2}^2 + \nu \|\nabla \mathbf{e}_h\|_{\mathbf{L}^2}^2 \\ & \leq \nu \|\nabla[\mathbb{S}_h(\mathbf{u}) - \mathbb{P}_h(\mathbf{u})]\|_{\mathbf{L}^2}^2 + \left( \frac{1}{T} + 4 \|\nabla \mathbb{P}_h(\mathbf{u})\|_{\mathbf{L}^\infty} \right) \|\mathbf{e}_h\|_{\mathbf{L}^2}^2 + 3T \|\nabla[p - L_h(p)]\|_{\mathbf{L}^2}^2 \\ & \quad + 3T \left( \|\mathbb{P}_h(\mathbf{u})\|_{\mathbf{L}^\infty}^2 \|\nabla \cdot \mathbb{P}_h(\mathbf{u})\|_{\mathbf{L}^2}^2 + 2 \|\nabla \mathbb{P}_h(\mathbf{u})\|_{\mathbf{L}^\infty}^2 \|\mathbf{u} - \mathbb{P}_h(\mathbf{u})\|_{\mathbf{L}^2}^2 + 2 \|\mathbf{u}\|_{\mathbf{L}^\infty}^2 \|\nabla[\mathbf{u} - \mathbb{P}_h(\mathbf{u})]\|_{\mathbf{L}^2}^2 \right). \end{aligned}$$

Similarly as in the pressure-robust case, Gronwall's lemma concludes the proof.  $\blacksquare$

## 5 Consistency errors and the accuracy of low/high-order methods

The main argument of this contribution is that pressure-robust space discretisations allow to reduce the (formal) approximation order of the algorithms, without compromising the accuracy, since the discrete Helmholtz–Hodge projector  $\|\mathbb{P}_h(\nabla p)\|_{\mathbf{L}^2}$  of classical, non-pressure-robust discretisations suffers from a consistency error. This section will now interpret the numerical analysis of Section 4 according to this point of view. The main difference between Theorems 4.1 (pressure-robust) and 4.5 (non-pressure-robust) is the term

$$3T \|\nabla[p - L_h(p)]\|_{\mathbf{L}^2(\mathbf{L}^2)} \quad (31)$$

in the  $\mathbf{L}^2$  estimate for the non-pressure-robust error  $\mathbf{e}_h$ , which is a direct consequence of the consistency error  $\|\mathbb{P}_h(\nabla p)\|_{\mathbf{L}^2}$  in Lemma 3.14.

In the following, let  $k_{\mathbf{u}}^{\text{cl}}/k_p^{\text{cl}}$  be the order of the discrete velocity/pressure polynomials for a classical, non-pressure robust method and, analogously,  $k_{\mathbf{u}}^{\text{pr}}/k_p^{\text{pr}}$  the orders for a pressure-robust FE discretisation.

### 5.1 Lowest-order discretisations

An obvious, seemingly yet unknown conclusion from (31) is that for non-pressure-robust space discretisations, for  $k_p^{\text{cl}} = 0$  no convergence order at all can be expected on pre-asymptotic meshes in presence of non-negligible pressures  $p$ . The reason is simple: discrete  $\mathbb{P}_0$  pressure do not have any approximation property w.r.t. the  $H^1$  norm of  $p$ .

Recently, in [42] it was numerically confirmed that the estimate (31) is sharp. The discretely inf-sup stable, non-pressure-robust Crouzeix–Raviart element indeed shows an error behaviour  $\mathbf{e}_h = \mathcal{O}(1)$  on pre-asymptotic meshes for  $\nu \ll 1$ , i.e., no convergence order at all was observed — a classical locking phenomenon. Furthermore, in the time-dependent Stokes problem, it was shown that classical, non-pressure-robust methods with  $k_p^{\text{cl}} = k_{\mathbf{u}}^{\text{cl}} - 1$  even lose two orders of convergence in the  $\mathbf{L}^2$  norm w.r.t. comparable pressure-robust methods. E.g., while the pressure-robust Scott–Vogelius element with  $(k_{\mathbf{u}}^{\text{pr}} = 2, k_p^{\text{pr}} = 1)$  converges with the optimal order 3 in the  $\mathbf{L}^2$  norm, the classical, non-pressure-robust Taylor–Hood method  $(k_{\mathbf{u}}^{\text{cl}} = 2, k_p^{\text{cl}} = 1)$  converges only with order 1 in the  $\mathbf{L}^2$ -norm [42].

Thus, non-pressure-robust space discretisations need higher-order discrete pressure spaces in order to get reasonable convergence orders for their discrete velocities — since high-order discrete pressure approximations reduce the consistency error  $\|\mathbb{P}_h(\nabla p)\|_{\mathbf{L}^2}$  by a simple Taylor expansion. Due to inf-sup stability, usually it holds  $k_{\mathbf{u}}^{\text{cl}} \geq k_p^{\text{cl}}$  (usually  $k_p^{\text{cl}} = k_{\mathbf{u}}^{\text{cl}} - 1$ ), and high-order discrete pressure spaces require high-order discrete velocity spaces as well. As a conclusion, pressure-robust methods with  $k_p^{\text{pr}} = k_{\mathbf{u}}^{\text{pr}} - 1$  for the time-dependent Stokes problem converge with two more orders of convergence in the  $\mathbf{L}^2$  norm than non-pressure-robust methods with  $k_p^{\text{cl}} = k_{\mathbf{u}}^{\text{cl}} - 1$ , if the pressure  $\nabla p$  is non-negligible [42].

## 5.2 Beltrami flows

The considerations for time-dependent Stokes problems with  $\nu \ll 1$  and large pressure gradients  $\nabla p$  are now applied to high-Reynolds number Beltrami flows, where it holds  $\mathbf{f} = \mathbf{0}$  and  $-(\mathbf{u} \cdot \nabla)\mathbf{u} = -\frac{1}{2}\nabla|\mathbf{u}|^2 = \nabla p$ , i.e., the dominant nonlinear convection term induces a large pressure gradient.

### 5.2.1. Polynomial potential flows

A simple consideration allows to show that pressure-robust discretisations sometimes allow to reduce the formal approximation order from  $k_{\mathbf{u}}^{\text{cl}} = 2k + 1$  (non-pressure-robust,  $k_p^{\text{cl}} = k_{\mathbf{u}}^{\text{cl}} - 1$ ) to  $k_{\mathbf{u}}^{\text{pr}} = k$  without compromising the accuracy for the discrete velocities at all.

Let us assume that for all  $t \in [0, T]$ ,  $(\mathbf{u}, p)$  is a time-dependent polynomial potential flow with  $h(t) \in \mathbb{P}_{k+1}$  for all  $t$ , i.e., it holds for all times that  $\mathbf{u}(t) = \nabla h(t)$ ,  $\nabla p(t) = -\frac{1}{2}\nabla|\mathbf{u}(t)|^2$  and  $\Delta h(t) = 0$ . Then,  $(\mathbf{u}(t), p(t)) \in \mathbb{P}_k \times \mathbb{P}_{2k}$  fulfils (for all fixed  $\nu > 0$ ) the time-dependent Navier–Stokes equations (1) with  $\mathbf{f} = \mathbf{0}$ , and  $\mathbf{u}$  is indeed a Beltrami flow, see Section 2. Note that one has to impose, e.g., time-dependent inhomogeneous Dirichlet velocity boundary conditions. A pressure-robust space discretisation of order  $k_{\mathbf{u}}^{\text{pr}} = k$  will deliver the exact velocity solution  $\mathbf{u}_h(t) = \mathbf{u}(t)$  for all  $t \in [0, T]$  according to Theorem 4.1 on every shape-regular mesh. On the contrary, non-pressure-robust space discretisations only deliver the exact velocity solution  $\mathbf{u}_h(t) = \mathbf{u}(t)$ , if it also holds  $p(t) \in Q_h$  for all  $t \in [0, T]$  according to the consistency error (31) in Theorem 4.5. Thus, classical space discretisations (with  $k_p^{\text{cl}} = k_{\mathbf{u}}^{\text{cl}} - 1$ ) require  $k_p^{\text{cl}} = 2k$ , i.e.,  $k_{\mathbf{u}}^{\text{cl}} = k_p^{\text{cl}} + 1 = 2k + 1$ .

This observation has been already published in [39]. Therefore, we simply refer to the numerical results therein.

### 5.2.2. Non- $C^\infty$ Beltrami flows

In the following, it is assumed that  $\mathbf{u}$  is a time-dependent Beltrami flow with  $\mathbf{u} \in L^\infty(0, T; \mathbf{H}^{k+1})$  for  $k \in \mathbb{N}$  and  $k \geq 1 + d/2$  and  $\mathbf{u} \notin L^\infty(0, T; \mathbf{H}^{k+1+\varepsilon})$  for any  $\varepsilon > 0$ . According to Theorem 4.1 for  $\nu \ll 1$ , one gets for pressure-robust space discretisations with  $k_{\mathbf{u}}^{\text{pr}} = k$  a convergence order  $k \leq k_{\mathbf{u}}^{\text{pr}} \leq k + 1$  for the  $\mathbf{L}^2$  norm; note that the nonlinearity of the problem may lead to a reduction of the convergence order on pre-asymptotic meshes, as compared to the time-dependent Stokes problem [40].

Turning to non-pressure-robust methods, one notes that due to  $\nabla p = -\frac{1}{2}\nabla|\mathbf{u}|^2$  and  $\mathbf{u} \in L^\infty(0, T; \mathbf{H}^{k+1})$  it holds  $p \in L^\infty(0, T; H^{k+1})$ . The result can be proven by the Leibniz formula yielding for the  $\kappa$ -th derivative of  $\frac{1}{2}(f(x))^2$  (with  $\kappa = 0, 1, \dots, k + 1$ )

$$\frac{1}{2}|(f(x))^2|^{(\kappa)} = \frac{1}{2} \sum_{i=0}^{\kappa} \binom{\kappa}{i} f^{(\kappa-i)} f^{(i)}. \quad (32)$$

According to the Sobolev imbedding theorem for  $d \leq 3$ , one concludes: for  $f \in H^1$  it holds also  $f \in L^6$  and for  $f \in H^2$  it holds also  $f \in L^\infty$ . Therefore, all the terms in (32) are either in  $L^3$  or in  $L^2$ , if at least  $f \in H^2$ . Substituting  $f = |\mathbf{u}|$  and searching for partial derivatives delivers the regularity for the pressure  $p$ . Due to the spatial regularity  $(\mathbf{u}, p) \notin \mathbf{H}^{k+1+\varepsilon} \times H^{k+1+\varepsilon}$ , one concludes that any space discretisation method with  $k_{\mathbf{u}}^{\text{cl}} > k$  cannot converge with a better convergence order than the pressure-robust method with  $k_{\mathbf{u}}^{\text{pr}} = k$ .



Also the pressure-dependent velocity error contribution (31) has a consistency error, which cannot be expected to be better than of order  $k$ .

Prescribing a certain accuracy of the velocity error of the pressure-robust method like

$$\|\mathbf{e}_h\|_{L^\infty(0,T;\mathbf{L}^2)} \leq \frac{\varepsilon}{\|\mathbf{u}\|_{L^\infty(0,T;\mathbf{L}^2)}}$$

for  $\mathbf{u} \neq \mathbf{0}$  and  $\varepsilon \ll 1$  can be fulfilled for mesh sizes  $h$  which are fine enough, i.e.,  $h < h(\varepsilon)$ ; in the case  $\mathbf{u}(t) \equiv \mathbf{0}$ , every mesh allows for the exact solution  $\mathbf{u}_h(t) = \mathbf{u}(t)$  for pressure-robust methods. Now, the solution  $\mathbf{u}$  can be represented as  $\mathbf{u} = \mathbf{u}_h + (\mathbf{u} - \mathbf{u}_h) =: \mathbf{u}_h + \mathbf{r}$ .

Then, it holds further  $\nabla p = -\nabla(\frac{1}{2}|\mathbf{u}_h|^2 + \mathbf{u}_h \cdot \mathbf{r} + \frac{1}{2}|\mathbf{r}|^2)$  with  $\mathbf{r} \in L^\infty(0,T;\mathbf{H}^{k+1})$ ,  $\frac{1}{2}|\mathbf{r}|^2 \in L^\infty(0,T;\mathbf{H}^{k+1})$  and  $\|\mathbf{r}\|_{L^\infty(0,T;\mathbf{L}^2)} \approx \varepsilon/\|\mathbf{u}\|_{L^\infty(0,T;\mathbf{L}^2)}$ . Due to  $\frac{1}{2}|\mathbf{u}_h|^2 \in \mathbb{P}_{2k}(\mathcal{T}_h)$  one can get (depending on the flow field  $\mathbf{u}$  and its Sobolev seminorms  $|\mathbf{u}|_{\mathbf{H}^i}$  for  $i = 0, 1, \dots, 2k-1$ ) that the approximation of  $\frac{1}{2}|\mathbf{u}_h|^2$  by piecewise polynomials from  $\mathbb{P}_i(\mathcal{T}_h)$  may lead to a non-negligible error for all  $i = 0, 1, \dots, 2k-1$ . Note that the higher derivatives of  $-\frac{1}{2}|\mathbf{u}|^2$  are given by a weighted sum of products of low- and high-order derivatives of  $\mathbf{u}$  according to (32). Then, only the choice  $k_p^{\text{cl}} = 2k$  and  $k_u^{\text{cl}} = 2k+1$  can ensure that for the classical, non-pressure-robust method also holds  $\|\nabla[p - L_h(p)]\|_{L^2(\mathbf{L}^2)} = \mathcal{O}(\varepsilon)$ .

Thus, the considerations for purely polynomial Beltrami flows can also be extended to more general Beltrami flows, and pressure-robust discretisations of formal order  $k_u^{\text{pr}} = k$  can be comparably accurate as classical, non-pressure-robust discretisations of order  $k_u^{\text{cl}} = 2k+1$ .

### 5.2.3. Analytic Beltrami flows

For analytic, but non-polynomial Beltrami flows no clear statements beyond Subsection 5.1 can be given about how much pressure-robust methods allow to reduce the formal order of the approximations without compromising the accuracy. However, in the numerical examples below we will exclusively compare numerical results on analytic flows, where high-order methods profit from exponential convergence. Nevertheless, one can confirm that for moderate formal approximation orders up to  $k_u^{\text{cl}} = 6$  pressure-robust methods allow for halving the approximation order without compromising the accuracy on coarse meshes.

### 5.3 Generalised Beltrami flows

Actually, pure Beltrami flows are only difficult for classical, non-pressure-robust space discretisations whenever the nonlinear convection term is approximated by the so-called convective form  $(\mathbf{u}_h \cdot \nabla)\mathbf{u}_h$  (or a skew-symmetric variant thereof). Alternatively, one can exploit (10) which tells us that it holds

$$\mathbb{P}((\mathbf{u} \cdot \nabla)\mathbf{u}) = \mathbb{P}((\nabla \times \mathbf{u}) \times \mathbf{u}). \quad (33)$$

Therefore, velocity solutions of the incompressible Navier–Stokes equations (1) also fulfil

$$\partial_t \mathbf{u} - \nu \Delta \mathbf{u} + (\nabla \times \mathbf{u}) \times \mathbf{u} + \nabla \pi^{\text{rot}} = \mathbf{f}, \quad \nabla \cdot \mathbf{u} = 0,$$

where the pressure  $p$  has been replaced by the new pressure variable

$$\pi^{\text{rot}} := p + \frac{1}{2} \nabla |\mathbf{u}|^2. \quad (34)$$

This is the so-called rotational or vector-invariant form [43] of the incompressible Navier–Stokes equations which is equivalent to the convective form.

It should be noted that pressure-robust (exactly divergence-free) methods, like the Scott–Vogelius element, deliver exactly the same discrete velocities for the convective and the rotational form on every mesh, since

they appropriately handle the equivalence classes of forces leading to (33) [11]. On the other hand, classical, non-pressure robust methods, which do not respect the equivalence classes of forces exactly, deliver different discrete velocities. For Beltrami flows, one obtains

$$\pi^{\text{rot}} = -\frac{1}{2}\nabla|\mathbf{u}|^2 + \frac{1}{2}\nabla|\mathbf{u}|^2 = 0$$

and the issue of a lack of pressure-robustness in classical space discretisations does not play any role for high Reynolds number Beltrami flows using the the rotational form of the Navier–Stokes equations [39].

So, why not simply using classical, non-pressure-robust methods in connection with the rotational form for the simulation of high Reynolds number flows? The reason is that there exist generalised Beltrami flows, — where  $(\mathbf{u} \cdot \nabla)\mathbf{u}$  is a gradient field — which can be accurately simulated with classical methods with the convective form, but not accurately with the rotational form at high Reynolds numbers. We also refer to e.g. [56] for numerical investigations showing that the rotational form of the incompressible Navier–Stokes can be inaccurate in FEM discretisations.

The easiest example is quadratic, planar Hagen–Poiseuille flow in a channel. Here, it holds  $(\mathbf{u} \cdot \nabla)\mathbf{u} = \mathbf{0}$ , and the nonlinear convection term is a trivial gradient field, which is, e.g., always a discrete solution of the non-pressure-robust Taylor–Hood element  $\mathbb{P}_2/\mathbb{P}_1$  for all Reynolds numbers on all meshes. However, using the quadratic Taylor–Hood element in connection with the rotational form will lead to enormous velocity errors on coarse meshes and high Reynolds numbers, since the corresponding pressure  $\pi^{\text{rot}}$  will be a fourth order polynomial, again.

Moreover, in complicated flows like in a Kármán vortex street, see Section 8, usually there dominate different generalised Beltrami flows locally: at the inlet a situation similar to a Hagen–Poiseuille flow dominates, where the convective form is accurate for classical discretisations, and around the obstacle a situation like a Beltrami flow prevails — where the rotational form is more accurate for classical discretisations.

In conclusion, pressure-robust discretisations respect (33) exactly on the discrete level and are thus appropriate for all types of situations. However, if for a generalised Beltrami flow the classical discretisation in convective form is compared to a pressure-robust discretisation, the pressure-robust discretisation may have a dramatic speedup (for Beltrami-type flows), but it can also happen that there is no speedup at all, since Hagen–Poiseuille with the trivial nonlinear convection term  $(\mathbf{u} \cdot \nabla)\mathbf{u} = \mathbf{0}$  is also a generalised Beltrami flow. Thus, the speedup question is not really decidable, but large speedups are achievable for generalised Beltrami flows, see, e.g., the numerical results in Subsection 7.1.

## 6 $H(\text{div})$ - and $L^2$ -DG finite element methods

In order to illustrate the numerical analysis developed in Section 4, we will present several numerical studies that compare pressure-robust versus classical, non-pressure-robust space discretisations. In order to make a fair and convincing comparison we will perform the numerical benchmarks from now on with Discontinuous Galerkin (DG) methods. The reason for this choice is manifold. First and most important, with the software package `NGSolve` [49], there exists a versatile, well-established and efficient numerical implementation of plenty of different DG methods, allowing especially for high-order space discretisation.

We choose to compare an exactly divergence-free, pressure-robust  $H(\text{div})$ -conforming DG method with a classical, non-pressure-robust DG methods which is only  $L^2$ -conforming (both discretely inf-sup stable). In this setting, our second reason for using DG methods is that after choosing elementwise polynomials of order  $k_{\mathbf{u}}$  for the velocity, both the  $H(\text{div})$ - and the  $L^2$ -DG method work with the same (discontinuous) discrete pressure space of polynomial order  $k_p = k_{\mathbf{u}} - 1$ . Thus, both methods have a roughly comparable number of

degrees of freedom and we think that a comparison between these methods is quite fair.

Third, we will deal with flows at high Reynolds numbers which makes a certain convection stabilisation desirable and/or necessary. In the DG context, upwind techniques are well-established and  $\mathbf{H}(\text{div})$ - and  $\mathbf{L}^2$ -conforming DG methods allow to apply exactly the same upwind stabilisation, facilitating a fair comparison. In Figure 2 the (moderately) positive effect w.r.t. the numerical error of a upwind stabilised versus a centred discretisation of the convection term is illustrated — which is not at all self-evident for generalised Beltrami flows, by the way.

Last but not least, we emphasise that a similar numerical analysis as in the case of  $\mathbf{H}^1$ -conforming space discretisations is possible for DG methods as well, but would only involve additional technical problems due to the facet terms required for DG discretisations. Instead, the issue of pressure-robustness in DG methods is described in this section. Again, one has to investigate the consistency errors of appropriately defined discrete Helmholtz–Hodge projectors for  $\mathbf{H}(\text{div})$ - and  $\mathbf{L}^2$ -conforming DG methods in the  $\mathbf{L}^2$  norm. In fact, their behaviour is exactly the same as in the context of  $\mathbf{H}^1$ -conforming methods, analysed in Theorems 4.1 and 4.5.

### 6.1 DG formulation

Beginning with the standard setting in DG methods [47, 18], let  $\mathcal{T}_h$  be a shape-regular FE partition (for brevity, we restrict ourselves to simplicial meshes in this work) of  $\Omega$  without hanging nodes and mesh size  $h = \max_{K \in \mathcal{T}_h} h_K$ , where  $h_K$  denotes the diameter of the particular element  $K \in \mathcal{T}_h$ . The skeleton  $\mathcal{F}_h$  denotes the set of all facets of  $\mathcal{T}_h$ ,  $\mathcal{F}_K = \{F \in \mathcal{F}_h : F \subset \partial K\}$  and  $h_F$  represents the diameter of each facet  $F \in \mathcal{F}_h$ . Moreover,  $\mathcal{F}_h = \mathcal{F}_h^i \cup \mathcal{F}_h^\partial$  where  $\mathcal{F}_h^i$  is the subset of interior facets and  $\mathcal{F}_h^\partial$  collects all Dirichlet boundary facets  $F \subset \partial\Omega$ . Facets lying on a periodic surface of  $\partial\Omega$  are treated as interior facets. To any  $F \in \mathcal{F}_h$  we assign a unit normal vector  $\mathbf{n}_F$  where, for  $F \in \mathcal{F}_h^\partial$ , this is the outer unit normal vector  $\mathbf{n}$ . If  $F \in \mathcal{F}_h^i$ , there are two adjacent elements  $K^+$  and  $K^-$  sharing the facet  $F = \partial K^+ \cap \partial K^-$  and  $\mathbf{n}_F$  points in an arbitrary but fixed direction. Let  $\phi$  be any piecewise smooth (scalar-, vector- or matrix-valued) function with traces from within the interior of  $K^\pm$  denoted by  $\phi^\pm$ , respectively. Then, we define the jump  $[[\cdot]]_F$  and average  $\{\!\!\{ \cdot \}\!\!\}_F$  operator across interior facets  $F \in \mathcal{F}_h^i$  by

$$[[\phi]]_F = \phi^+ - \phi^- \quad \text{and} \quad \{\!\!\{ \phi \}\!\!\}_F = \frac{1}{2}(\phi^+ + \phi^-). \quad (35)$$

For boundary facets  $F \in \mathcal{F}_h^\partial$  we set  $[[\phi]]_F = \{\!\!\{ \phi \}\!\!\}_F = \phi$ . These operators act componentwise for vector- and matrix-valued functions. Frequently, the subscript indicating the facet is omitted.

Let  $\mathbf{V}_h/Q_h$  be the considered discretely inf-sup stable velocity/pressure (discontinuous) FE pair. In order to approximate (15), the following generic semi-discrete DG method is considered:

$$\begin{cases} \text{Find } (\mathbf{u}_h, p_h) : (0, T] \rightarrow \mathbf{V}_h \times Q_h \text{ with } \mathbf{u}_h(0) = \mathbf{u}_{0h} \text{ s.t., } \forall (\mathbf{v}_h, q_h) \in \mathbf{V}_h \times Q_h, & (36a) \\ (\partial_t \mathbf{u}_h, \mathbf{v}_h) + \nu a_h(\mathbf{u}_h, \mathbf{v}_h) + c_h(\mathbf{u}_h; \mathbf{u}_h, \mathbf{v}_h) + b_h(\mathbf{v}_h, p_h) + b_h(\mathbf{u}_h, q_h) & (36b) \\ = (\mathbf{f}, \mathbf{v}_h) + \nu a_h^\partial(\mathbf{g}_D; \mathbf{v}_h) + c_h^\partial(\mathbf{g}_D; \mathbf{u}_h, \mathbf{v}_h) + b_h^\partial(\mathbf{g}_D, q_h). & (36c) \end{cases}$$

Here,  $\mathbf{u}_{0h}$  denotes a suitable approximation of the initial velocity  $\mathbf{u}_0$ . In the following, based on [47, 18], we introduce the various terms which appear in (36). Note that only the particular choice of the discrete velocity space  $\mathbf{V}_h$  will distinguish the pressure-robust from the non-pressure-robust method in the end.

Denote the broken gradient by  $\nabla_h$ . For the discretisation of the diffusion term, we choose the symmetric

interior penalty method with a sufficiently large penalisation parameter  $\sigma > 0$ :

$$a_h(\mathbf{u}_h, \mathbf{v}_h) = \int_{\Omega} \nabla_h \mathbf{u}_h : \nabla_h \mathbf{v}_h \, d\mathbf{x} + \sum_{F \in \mathcal{F}_h} \frac{\sigma}{h_F} \oint_F \llbracket \mathbf{u}_h \rrbracket \cdot \llbracket \mathbf{v}_h \rrbracket \, ds \quad (37a)$$

$$- \sum_{F \in \mathcal{F}_h} \oint_F \{ \nabla_h \mathbf{u}_h \} \mathbf{n}_F \cdot \llbracket \mathbf{v}_h \rrbracket \, ds - \sum_{F \in \mathcal{F}_h} \oint_F \llbracket \mathbf{u}_h \rrbracket \cdot \{ \nabla_h \mathbf{v}_h \} \mathbf{n}_F \, ds \quad (37b)$$

$$a_h^\partial(\mathbf{g}_D; \mathbf{v}_h) = \sum_{F \in \mathcal{F}_h^\partial} \frac{\sigma}{h_F} \oint_F \mathbf{g}_D \cdot \mathbf{v}_h \, ds - \sum_{F \in \mathcal{F}_h^\partial} \oint_F \mathbf{g}_D \cdot (\nabla_h \mathbf{v}_h) \mathbf{n}_F \, ds \quad (37c)$$

Using the broken divergence  $\nabla_h \cdot$ , the pressure-velocity coupling is realised by

$$b_h(\mathbf{u}_h, q_h) = - \int_{\Omega} q_h (\nabla_h \cdot \mathbf{u}_h) \, d\mathbf{x} + \sum_{F \in \mathcal{F}_h} \oint_F (\llbracket \mathbf{u}_h \rrbracket \cdot \mathbf{n}_F) \{ q_h \} \, ds, \quad (38a)$$

$$b_h^\partial(\mathbf{g}_D; q_h) = \sum_{F \in \mathcal{F}_h^\partial} \oint_F (\mathbf{g}_D \cdot \mathbf{n}) q_h \, ds. \quad (38b)$$

For the nonlinear inertia term, we decide to use the following skew-symmetrised (upwind) discretisation in convection form:

$$c_h(\mathbf{w}_h; \mathbf{u}_h, \mathbf{v}_h) = \int_{\Omega} (\mathbf{w}_h \cdot \nabla_h) \mathbf{u}_h \cdot \mathbf{v}_h \, d\mathbf{x} + \frac{1}{2} \int_{\Omega} (\nabla_h \cdot \mathbf{w}_h) \mathbf{u}_h \cdot \mathbf{v}_h \, d\mathbf{x} \quad (39a)$$

$$- \sum_{F \in \mathcal{F}_h^i} \oint_F (\{ \mathbf{w}_h \} \cdot \mathbf{n}_F) \llbracket \mathbf{u}_h \rrbracket \cdot \{ \mathbf{v}_h \} \, ds - \frac{1}{2} \sum_{F \in \mathcal{F}_h} \oint_F (\llbracket \mathbf{w}_h \rrbracket \cdot \mathbf{n}_F) \{ \mathbf{u}_h \cdot \mathbf{v}_h \} \, ds \quad (39b)$$

$$+ \sum_{F \in \mathcal{F}_h^i} \oint_F \frac{\theta}{2} \{ \mathbf{w}_h \} \cdot \mathbf{n}_F \llbracket \mathbf{u}_h \rrbracket \cdot \llbracket \mathbf{v}_h \rrbracket \, ds \quad (39c)$$

$$c_h^\partial(\mathbf{g}_D; \mathbf{u}_h, \mathbf{v}_h) = - \frac{1}{2} \sum_{F \in \mathcal{F}_h^\partial} \oint_F (\mathbf{g}_D \cdot \mathbf{n}) (\mathbf{u}_h \cdot \mathbf{v}_h) \, ds \quad (39d)$$

Here, the parameter  $\theta \in \{0, 1\}$  decides whether the considered method term uses an upwind stabilisation ( $\theta = 1$ ) for the convection term or not ( $\theta = 0$ ).

Concerning the particular choice of FE spaces, let  $\mathbb{P}_k(K)$  denote the local space of all polynomials on  $K$  with degree less or equal to  $k$ . Then, given  $k \geq 2$ , the pressure space for both the  $\mathbf{H}(\text{div})$ - and the  $\mathbf{L}^2$ -DG method coincides:

$$Q_h = \{ q_h \in L_0^2(\Omega) : q_h|_K \in \mathbb{P}_{k-1}(K), \forall K \in \mathcal{T}_h \}, \quad (40)$$

i.e., it holds  $k_p = k - 1$ . While the discrete pressure spaces for the  $\mathbf{H}(\text{div})$ - and  $\mathbf{L}^2$  conforming DG methods are the same, the velocity spaces, however, differ. Recalling

$$\mathbf{H}(\text{div}; \Omega) = \{ \mathbf{v} \in \mathbf{L}^2(\Omega) : \nabla \cdot \mathbf{v} \in L^2(\Omega) \},$$

the FE velocity spaces are defined as follows:

$$\mathbf{H}(\text{div})\text{-DG:} \quad \mathbf{V}_h = \{ \mathbf{v}_h \in \mathbf{H}(\text{div}; \Omega) : \mathbf{v}_h|_K \in \mathbb{P}_k(K), \forall K \in \mathcal{T}_h; (\mathbf{v}_h - \mathbf{g}_D) \cdot \mathbf{n}|_{\partial\Omega} = 0 \}, \quad (41a)$$

$$\mathbf{L}^2\text{-DG:} \quad \mathbf{V}_h = \{ \mathbf{v}_h \in \mathbf{L}^2(\Omega) : \mathbf{v}_h|_K \in \mathbb{P}_k(K), \forall K \in \mathcal{T}_h \}. \quad (41b)$$

Note that the  $\mathbf{H}(\text{div})$  space is thus based on the Brezzi–Douglas–Marini element [10] and the resulting divergence-free DG method is strongly related to [16]. Finite element error analysis for the  $\mathbf{L}^2$ -DG method

can be found, for example, in [47, 18]. For the  $\mathbf{H}(\text{div})$ -DG method, we refer to [50]. In the DG setting, discretely divergence-free functions are defined using the pressure-velocity coupling  $b_h$  by

$$\mathbf{V}_h^{\text{div}} = \{\mathbf{v}_h \in \mathbf{V}_h : b_h(\mathbf{v}_h, q_h) = 0, \forall q_h \in Q_h\},$$

where we note that for the  $\mathbf{H}(\text{div})$  method,  $\mathbf{v}_h \in \mathbf{V}_h^{\text{div}}$  follows  $\nabla \cdot \mathbf{v}_h = 0$  pointwise.

**REMARK 6.1:** Deriving an analogous statement to Lemma 3.8 for DG methods is straightforward, but technically demanding. The necessary compactness arguments for DG methods are described in [18].

All computations in this work have been carried out with the high-order finite element library NGSolve [49].

## 6.2 Discrete DG Helmholtz–Hodge projectors

Every discretely inf-sup stable numerical method for the incompressible (Navier–)Stokes equations is intrinsically connected to a particular discrete Helmholtz–Hodge projector. The aim of this subsection is to investigate the properties of the discrete DG Helmholtz–Hodge projectors of the  $\mathbf{H}(\text{div})$ - and  $\mathbf{L}^2$ -DG methods. An analogous discussion for the discrete  $\mathbf{H}^1$  projectors has been done in Subsection 3.4.

The general definition of the discrete Helmholtz–Hodge projector  $\mathbb{P}_h$  of a function  $\mathbf{g} \in \mathbf{L}^2$  is given by

$$\mathbb{P}_h : \mathbf{L}^2(\Omega) \rightarrow \mathbf{V}_h^{\text{div}}, \quad \mathbb{P}_h(\mathbf{g}) = \arg \min_{\mathbf{v}_h \in \mathbf{V}_h^{\text{div}}} \|\mathbf{g} - \mathbf{v}_h\|_{\mathbf{L}^2(\Omega)}. \quad (42)$$

A suitable finite element method for this problem uses the already known pressure-velocity coupling form  $b_h$  and additionally, a mass bilinear form defined by  $m_h(\mathbf{u}_h, \mathbf{v}_h) = \int_{\Omega} \mathbf{u}_h \cdot \mathbf{v}_h \, d\mathbf{x}$ . The discrete weak form reads as follows:

$$\left\{ \begin{array}{l} \text{Find } (\mathbb{P}_h(\mathbf{g}), \phi_h) \in \mathbf{V}_h \times Q_h \text{ s.t., } \forall (\mathbf{v}_h, q_h) \in \mathbf{V}_h \times Q_h, \\ m_h(\mathbb{P}_h(\mathbf{g}), \mathbf{v}_h) + b_h(\mathbf{v}_h, \phi_h) + b_h(\mathbb{P}_h(\mathbf{g}), q_h) = (\mathbf{g}, \mathbf{v}_h). \end{array} \right. \quad (43a)$$

$$\quad (43b)$$

Now, choosing the discrete ‘velocity’ space according to the  $\mathbf{H}(\text{div})$ -DG choice (41a) leads to an exactly divergence-free discrete Helmholtz–Hodge projector called  $\mathbb{P}_h^{\text{div}}(\mathbf{g})$ . On the other hand, choosing  $\mathbf{V}_h$  according to the  $\mathbf{L}^2$ -DG choice (41b), the resulting discrete Helmholtz–Hodge projector is denoted by  $\mathbb{P}_h^0(\mathbf{g})$ . Note that while  $\nabla \cdot \mathbb{P}_h^{\text{div}}(\mathbf{g}) = 0$ , the  $\mathbf{L}^2$ -DG projector  $\mathbb{P}_h^0(\mathbf{g})$  is not divergence-free.

Let us now quantify the difference between these two discrete DG Helmholtz projectors more carefully. For the divergence-free  $\mathbf{H}(\text{div})$ -DG method, the analogue of Lemma 3.13 is the following.

### LEMMA 6.2

For the pressure-robust (divergence-free)  $\mathbf{H}(\text{div})$ -DG method, for all gradient fields  $\nabla\psi$  with  $\psi \in H^1(\Omega)$  it holds

$$\mathbb{P}_h(\nabla\psi) = \mathbf{0}.$$

**PROOF:** In this case, due to  $\mathbf{v}_h \in \mathbf{V}_h^{\text{div}}$  it follows  $\nabla \cdot \mathbf{v}_h = 0$  pointwise. Thus, for  $\nabla\psi \in \mathbf{L}^2(\Omega)$  it holds for all  $\mathbf{v}_h \in \mathbf{V}_h^{\text{div}}$ ,

$$(\nabla\psi, \mathbf{v}_h) = -(\psi, \nabla \cdot \mathbf{v}_h) = 0. \quad \blacksquare$$

For the non-pressure-robust  $\mathbf{L}^2$ -DG method, the analogue of Lemma 3.14 is again less favourable.

### LEMMA 6.3

For the non-pressure-robust  $\mathbf{L}^2$ -DG method, for all gradient fields  $\nabla\psi$  with  $\psi \in H^{k_p+1}(\Omega)$ , it holds

$$\|\mathbb{P}_h(\nabla\psi)\|_{\mathbf{L}^2(\Omega)} \leq Ch^{k_p} |\psi|_{H^{k_p+1}(\Omega)}. \quad (44)$$

**PROOF:** For all  $q \in H^1(\Omega)$  it holds for all  $\mathbf{v}_h \in \mathbf{V}_h^{\text{div}}$

$$(\nabla q, \mathbf{v}_h) = - \int_{\Omega} q(\nabla_h \cdot \mathbf{v}_h) \, d\mathbf{x} + \sum_{F \in \mathcal{F}_h} \oint_F q([\mathbf{v}_h] \cdot \mathbf{n}_F) \, ds = b_h(\mathbf{v}_h, q).$$

For  $L_h\psi \in H^1(\Omega) \cap Q_h$  it holds thus  $(\nabla(L_h\psi), \mathbf{v}_h) = 0$  due to (36), leading to

$$(\nabla\psi, \mathbf{v}_h) = (\nabla(\psi - L_h\psi), \mathbf{v}_h) \leq \|\nabla(\psi - L_h\psi)\|_{\mathbf{L}^2} \|\mathbf{v}_h\|_{\mathbf{L}^2}$$

and the result is proved like in the  $\mathbf{H}^1$ -conforming case in Lemma 3.14. ■

## 7 Numerical experiments with known exact solution

In this section, we use the previously described  $\mathbf{H}(\text{div})$ - and  $\mathbf{L}^2$ -DG methods to investigate incompressible flow problems at high Reynolds number where the exact solution is known to be a (generalised) Beltrami flow. The accuracy of the corresponding results is measured in the  $\mathbf{L}^2$  norm exclusively because the errors in  $\mathbf{H}^1$  do not provide any more insight.

### 7.1 2D planar lattice flow

Let us now compare the performance of the pressure-robust  $\mathbf{H}(\text{div})$ - and non-pressure-robust  $\mathbf{L}^2$ -DG methods in terms of accuracy and efficiency in a two-dimensional setting. In order to do so, we fix  $\nu = 10^{-6}$  and solve a problem with  $\mathbf{f} \equiv \mathbf{0}$ , where the exact solution is known and given by

$$\mathbf{u}_0(\mathbf{x}) = \begin{bmatrix} \sin(2\pi x_1) \sin(2\pi x_2) \\ \cos(2\pi x_1) \cos(2\pi x_2) \end{bmatrix}, \quad \mathbf{u}(t, \mathbf{x}) = \mathbf{u}_0(\mathbf{x}) e^{-8\pi^2 \nu t}. \quad (45)$$

We consider the domain  $\Omega = (0, 1)^2$  with periodic boundary conditions on all edges of  $\partial\Omega$  and compute until  $T = 10$ . The exact solution (45) is a classical example of a generalised Beltrami flow as the convective term  $(\mathbf{u} \cdot \nabla)\mathbf{u}$  balances the pressure gradient. For the simulation, only the initial velocity is prescribed according to  $\mathbf{u}_0$  and the evolution of the flow is observed. Varying orders  $k \in \{2, 3, 4, 6\}$  of the FE spaces with  $k_{\mathbf{u}} = k$  and  $k_p = k - 1$  are used and the resolution of the particular method is controlled via the mesh. We use unstructured triangular meshes for this 2D example and the SIP penalty parameter  $\sigma = (k + 1)(k + 2)$  is chosen, which has the correct quadratic  $k$ -dependency; see, for example, [31, Section 3.1].

The time-stepping is based on the second-order multistep implicit-explicit (IMEX) scheme SBDF2 [7] where the Stokes part of the problem is discretised implicitly with a BDF2 method and the convection part relies on an explicit treatment with second-order accurate extrapolation in time. The system matrix of the Stokes part is called  $M^*$  and note that in such an IMEX scheme, only linear system associated with  $M^*$  have to be solved in every time step. However, this particular time-stepping scheme is only a choice here and not crucial for the subsequent results. For the planar-lattice flow we use a constant time step of  $\Delta t = 10^{-4}$ .

We will compare the following two different quantities: total (velocity plus pressure) number of degrees of freedom (DOFs) and number of non-zero entries (NZE) of  $M^*$ . While the DOFs indicate how rich the approximation space is, the NZEs are a much more suitable measure of how efficient a particular discretisation is. The NZEs of  $M^*$  indicate how expensive solving linear systems is; usually, this is the most time consuming part of a flow solver (especially in 3D). In Figure 1, the corresponding  $L^2(0, T; \mathbf{L}^2(\Omega))$  errors can be seen for the two different methods introduced in Section 6.

Firstly, one can observe that whenever a fixed polynomial degree of the FE space is considered, the pressure-robust  $\mathbf{H}(\text{div})$ -FEM always leads to an at least ten times smaller error, both in terms of DOFs and NZEs. For higher-order and on finer meshes, this offset increases to such an extent that for  $k = 6$  the  $\mathbf{H}(\text{div})$ -DG

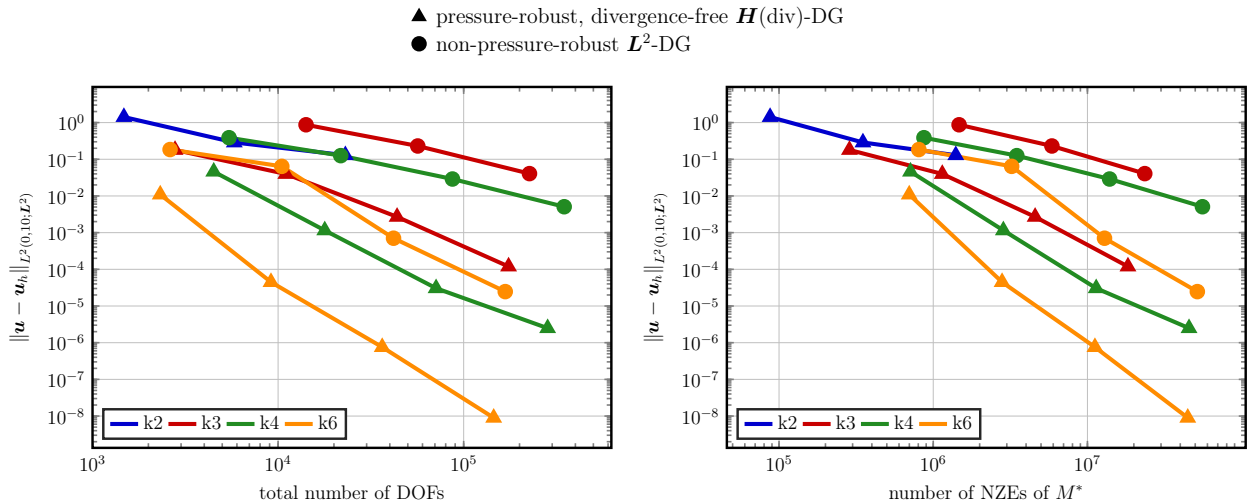


Figure 1:  $L^2(0, T; \mathbf{L}^2(\Omega))$  errors for the 2D lattice flow ( $\nu = 10^{-6}$ ). Comparison of pressure-robust  $\mathbf{H}(\text{div})$ - and non-pressure-robust  $L^2$ -DG methods with  $\Delta t = 10^{-4}$ , both using upwinding ( $\theta = 1$ ). The abscissae show the total number of DOFs (left) and number of NZEs of  $M^*$  (right).

method's solution has an error which is at least  $10^{-3}$  times smaller than the corresponding  $L^2$ -DG's. Even more remarkably, in terms of fixing DOFs, at least on coarse meshes the pressure-robust  $k = 2$   $\mathbf{H}(\text{div})$ -DG method results in a comparable accuracy as the  $k = 4$   $L^2$ -DG method while, at the same time, it leads to fewer NZEs. A similar observation holds for  $k = 3$   $\mathbf{H}(\text{div})$ -DG and  $k = 6$   $L^2$ -DG. In practice, as higher-order methods usually lead to more NZEs, being able to use a method of order  $k$  instead of  $2k$ , without losing accuracy, means a considerable improvement with respect to performance.

In Section 2, it was argued that the velocity solution  $\mathbf{u}$  of a generalised Beltrami flow is simultaneously a solution of the Navier–Stokes and the Stokes problem (only the pressures are different). We now want to consider, in a time-dependent setting, instead of the nonlinear Navier–Stokes problem with  $\mathbf{f} \equiv \mathbf{0}$ , the corresponding Stokes problem with  $\mathbf{f} = -(\mathbf{u} \cdot \nabla)\mathbf{u}$  solved with the pressure-robust  $\mathbf{H}(\text{div})$ -DG method for  $k = 6$ .

The evolution of  $L^2$  errors can be seen in Figure 2, where the left-hand side plot shows the behaviour of the Navier–Stokes solution with upwinding (solid lines) against the corresponding Stokes solution (dashed lines) for different refinement levels  $r_0, \dots, r_3$ . The main observations are that the Stokes error is a lower bound for the Navier–Stokes error at all times and that on sufficiently fine meshes, both errors are not too far apart. A second interesting issue is the question of the influence of upwinding on the solution. The right-hand side subfigure Figure 2 shows that upwinding is indeed helpful for this kind of convection dominated problems. More precisely, one can observe that the Navier–Stokes errors without upwinding (solid lines) are always larger than in the left-hand side subfigure. Also, upwinding seems to be especially important whenever the mesh is neither very coarse nor very fine.

## 7.2 Classical 3D Ethier–Steinman

Now, we want to repeat our investigation from Section 7.1 with a three-dimensional flow problem ( $\mathbf{f} \equiv \mathbf{0}$ ). Thus, consider the exact velocity of the Ethier–Steinman problem [22]:

$$\mathbf{u}_0(\mathbf{x}) = -a \begin{bmatrix} e^{ax_1} \sin(ax_2 + bx_3) + e^{ax_3} \cos(ax_1 + bx_2) \\ e^{ax_2} \sin(ax_3 + bx_1) + e^{ax_1} \cos(ax_2 + bx_3) \\ e^{ax_3} \sin(ax_1 + bx_2) + e^{ax_2} \cos(ax_3 + bx_1) \end{bmatrix}, \quad \mathbf{u}(t, \mathbf{x}) = \mathbf{u}_0(\mathbf{x})e^{-\nu a^2 t}. \quad (46)$$

Here, the parameters  $a = \pi/4$ ,  $b = \pi/2$  and  $\nu = 0.002$  are used and we are dealing with a Beltrami flow. As domain, the cube  $\Omega = (-1, 1)^3$  is chosen where the time-dependent Dirichlet boundary condition  $\mathbf{g}_D$

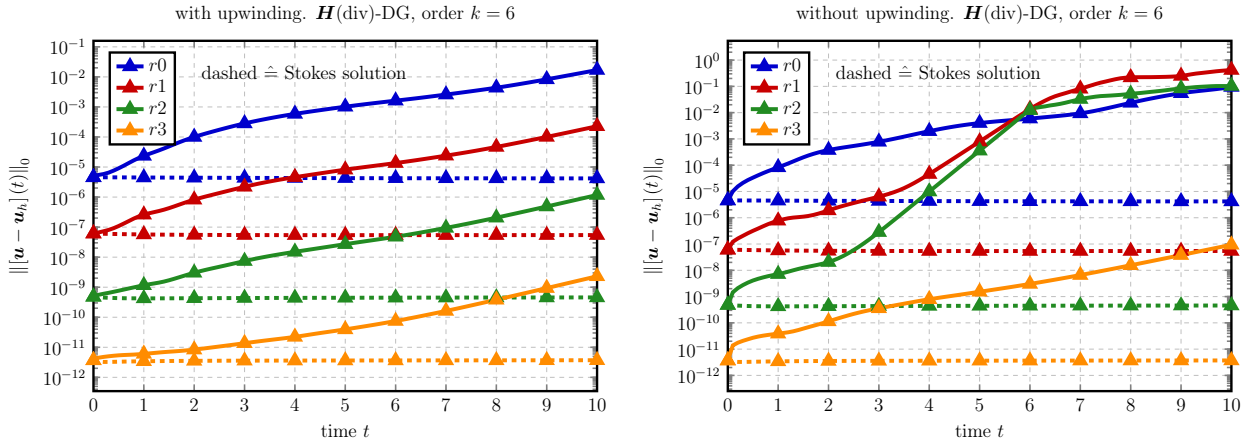


Figure 2: Evolution of  $L^2$  errors for the 2D lattice flow ( $\nu = 10^{-6}$ ). Comparison of pressure-robust  $\mathbf{H}(\text{div})$  solution ( $k = 6$ ) with  $\Delta t = 10^{-4}$  of the Navier–Stokes problem (solid lines) and the Stokes problem (dashed lines). The colours indicate different levels of mesh refinement. Navier–Stokes solution with upwinding  $\theta = 1$  (left), and without upwinding  $\theta = 0$  (right)

according to the exact solution is imposed. Again, the initial velocity  $\mathbf{u}_0$  is prescribed at  $t = 0$  and the evolution of the flow is observed. We stop the simulations at  $T = 1$  and the time-stepping is again based on the SBDF2 method, again using  $\Delta t = 10^{-4}$ . Unstructured tetrahedral meshes are used in the 3D example and the SIP penalty parameter  $\sigma = 8k^2$  is chosen. The resulting  $L^2(0, T; L^2(\Omega))$  errors can be seen in Figure 3.

Again, for each fixed  $k$ , the divergence-free and pressure-robust  $\mathbf{H}(\text{div})$ -DG method always yields the smallest errors. In terms of efficiency, the plot of the number of NZEs again shows that by using a pressure-robust method, a significant amount of computational effort can be saved. However, for sufficiently fine meshes, higher-order will always be superior because of the smoothness of the problem. The next section shall pick up at exactly this point.

### 7.3 3D Ethier–Steinman with inaccurate Dirichlet BCs

In applications, it is very rare that one has an exact geometry description of the underlying domain as, for example, curved boundaries make it necessary to approximate also the geometry to a certain accuracy. Therefore, the imposition of the *correct* Dirichlet BCs is usually made on the *approximated* boundary. Unavoidably, this is a source for errors and in this section we want to mimic such a situation in the following equivalent way. Instead of prescribing the correct Dirichlet BCs on the approximated boundary, we will impose inaccurate BCs on the correct boundary.

Let us revisit the 3D Ethier–Steinman example from Section 7.2. The exact solution is also given by (46), exactly the same parameters are used and again, time-dependent Dirichlet boundary conditions are imposed. However, as hinted at above, instead of choosing  $\mathbf{g}_D$  according to the exact solution  $\mathbf{u}$ , we will use a piecewise quadratic approximation of it instead. Figure 4 shows the resulting  $L^2(0, T; L^2(\Omega))$  errors.

First of all, note that the pressure-robust method is again always more accurate for a fixed number of DOFs and a fixed number of NZEs. In contrast to Section 7.2, the asymptotical behaviour for higher  $k$  and finer meshes is now, by construction, dominated by the accuracy of  $\mathbf{g}_D$ . Thus, one can see that all methods roughly lead to the same result when the resolution is high enough. More interestingly though, on coarse meshes, the pressure-robust method is always significantly more accurate.



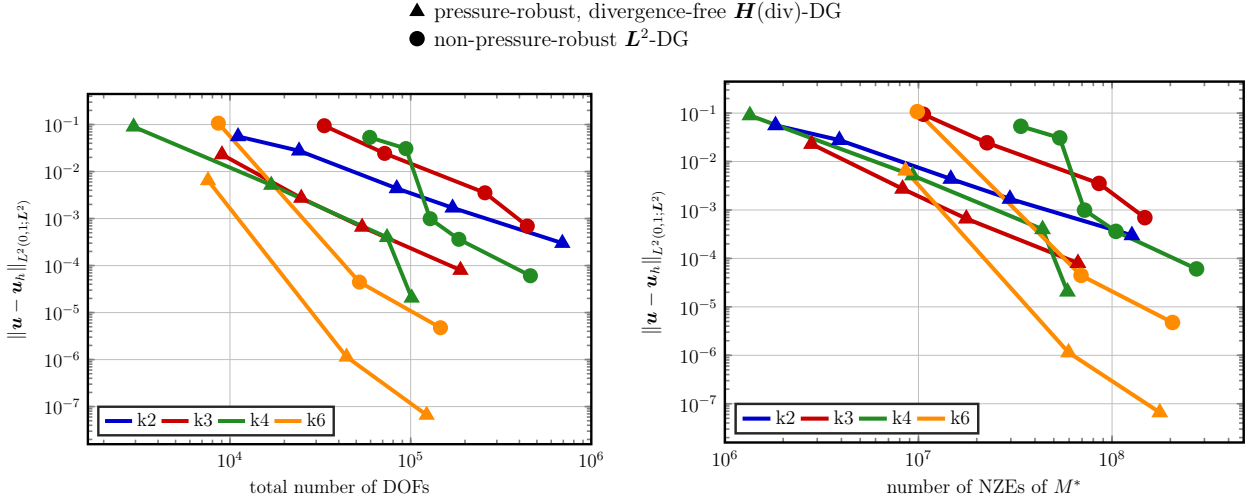


Figure 3: Errors for the classical 3D Ethier–Steinman problem ( $\nu = 0.002$ ). Comparison of pressure-robust  $\mathbf{H}(\text{div})$ - and non-pressure-robust  $L^2$ -DG methods with  $\Delta t = 10^{-4}$ , both using upwinding ( $\theta = 1$ ). The abscissae show the total number of DOFs (left) and number of NZEs of  $M^*$  (right).

## 8 Kármán vortex street — a generalised Beltrami flow?

Above it was shown that for generalised Beltrami flows, pressure-robust mixed methods can be much more accurate than classical mixed methods. However, a natural question is whether pressure-robust mixed methods are also superior for ‘real world flows’. Therefore, it is interesting to investigate to what extent real world flows are, at least in some parts of the domain, generalised Beltrami flows. For generalised Beltrami flows, the Helmholtz–Hodge projector of the nonlinear convection term, i.e.  $\mathbb{P}((\mathbf{u} \cdot \nabla)\mathbf{u})$ , vanishes, although  $(\mathbf{u} \cdot \nabla)\mathbf{u}$  itself does not vanish.

As an example of a practically relevant flow, let us consider the flow around an obstacle in a 2D channel of dimensions  $(L, H) = (3, 1.01)$ . Here, the obstacle is chosen as a square with side length  $r = 0.1$  whose lower left corner is placed at  $\mathbf{x} = (0.7, 0.45)^\dagger$ . In Figure 5, such a flow can be seen at a time instance where the characteristic vortex shedding of a periodic Kármán vortex street has formed. The Dirichlet inflow BC on the left part of the boundary is given by the parabolic profile  $u_1(t, 0, x_2) = 6x_2(H - x_2)/H^2$ , which, together with  $\nu = 10^{-3}$  leads to a Reynolds number  $Re = \bar{u}r/\nu = 1 \times 0.1 \times 1000 = 100$ . On top, bottom and the boundary of the square, no-slip is prescribed and the right part of the boundary represents the outflow boundary (do-nothing).

Being in this situation and having such a flow at hand, two main questions arise:

1. In which part of the domain does the flow behave like a generalised Beltrami flow?
2. Where locally does a pressure-robust method outperform a non-pressure robust one?

The most obvious approach for answering the first question is to begin with inspecting the convection term  $(\mathbf{u}_h \cdot \nabla)\mathbf{u}_h$  in a suitable norm. We have chosen to investigate it in the  $L^{3/2}$  norm, since even for 3D flows the nonlinear convection term is (for almost all times in the sense of Bochner spaces) in  $L^{3/2}$ .

Figure 6 shows such a qualitative approach where the divergence-free  $\mathbf{H}(\text{div})$ -DG method has been used. At first, we observe that in a large part of the domain the convective term (approximately) vanishes. Wherever

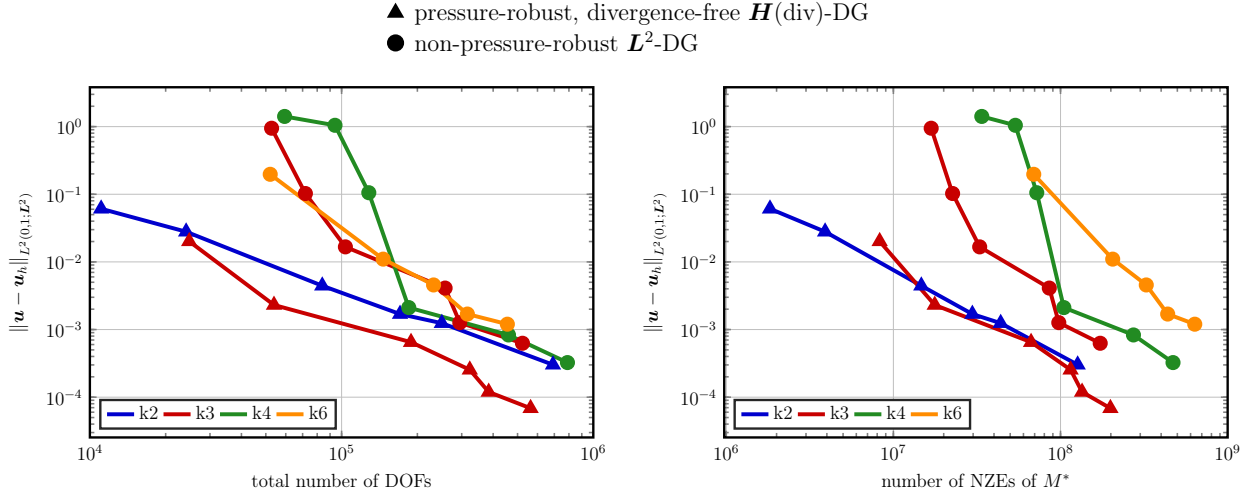


Figure 4: Errors for the 3D Ethier–Steinman problem ( $\nu = 0.002$ ) with inaccurate BCs. Comparison of pressure-robust  $\mathbf{H}(\text{div})$ - and non-pressure-robust  $L^2$ -DG methods with  $\Delta t = 10^{-4}$ , both using upwinding ( $\theta = 1$ ). The abscissae show the total number of DOFs (left) and number of NZEs of  $M^*$  (right).

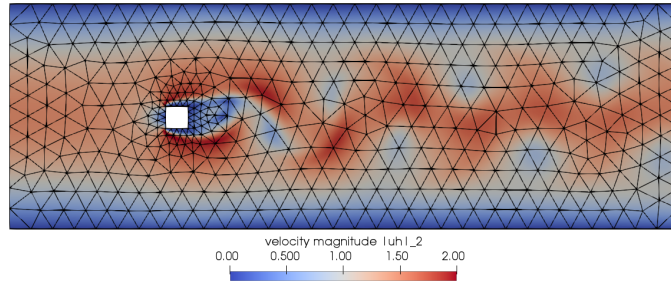


Figure 5: Periodic Kármán vortex shedding in the wake of a square. Visualisation of the velocity magnitude  $|\mathbf{u}_h|_2$ , the computational mesh and the underlying geometry. The computations are done with fourth-order elements ( $k = 4$ ) and upwinding ( $\theta = 1$ ), unless stated otherwise.

$(\mathbf{u}_h \cdot \nabla) \mathbf{u}_h \approx \mathbf{0}$ , the flow is locally a Stokes solution and thus trivially generalised Beltrami. According to the discussion in Subsection 5.3, for a non-pressure-robust method with the rotational form for the discrete nonlinear convection term, one can expect inaccurate results due to (10) in these parts of the domain since there it holds  $\boldsymbol{\omega} \times \mathbf{u} \approx -\frac{1}{2} \nabla |\mathbf{u}|^2$  which is a dominant gradient field whenever  $\mathbf{u}$  cannot be approximated by low-order polynomials. However, there are also some regions in the flow where the convection term itself is large (the upstream side of the obstacle and parts of the wake).

The more interesting question is, where  $\mathbf{f}_h = (\mathbf{u}_h \cdot \nabla) \mathbf{u}_h$  is locally a gradient. Thus, the gradient contribution of  $(\mathbf{u}_h \cdot \nabla) \mathbf{u}_h$  can be seen in Figure 7 where, for a better comparison, the colour bar scaling is chosen identically to that of Figure 6.

One can observe that especially in the direct vicinity of the obstacle, there is indeed a significant gradient contribution in  $(\mathbf{u}_h \cdot \nabla) \mathbf{u}_h$  which shows that a Kármán vortex street problem locally behaves like a generalised Beltrami flow. In the wake, however, the divergence-free contribution  $\mathbb{P}_h^{\text{div}}(\mathbf{f}_h)$  seems to dominate the dynamics of the convective part.

In order to answer the second question, namely where a pressure-robust method outperforms a non-pressure-

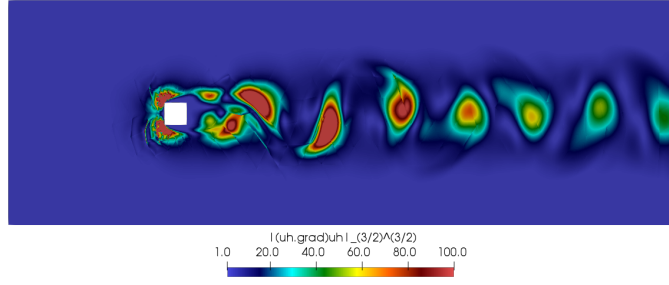


Figure 6: Discrete convection term  $|(\mathbf{u}_h \cdot \nabla)\mathbf{u}_h|_{3/2}^{3/2}$ . Note that the colour bar is chosen in such a way that values below unity are blue and everything above 100 is red.

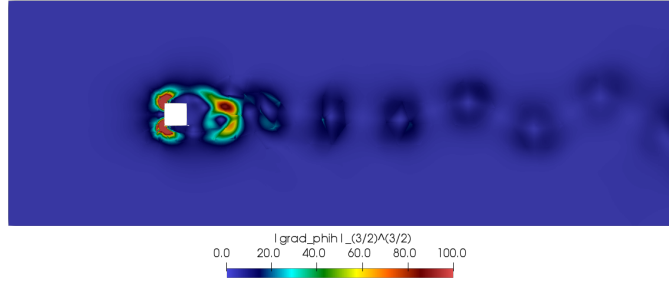


Figure 7: Gradient contribution  $|\nabla\phi_h|_{3/2}^{3/2}$  of discrete Helmholtz–Hodge decomposition with exactly divergence-free FEM. The colour bar scaling is chosen identically to that of Figure 6.

robust one, we solve a second discrete Helmholtz–Hodge decomposition problem of the form (43), but this time with the  $L^2$ -DG ‘velocity’ space choice (41b). Note again that due to using the  $L^2$ -DG method,  $\mathbb{P}_h^0(\mathbf{f}_h)$  is not exactly divergence-free, even though  $\mathbf{f}_h$  has been computed with the  $\mathbf{H}(\text{div})$ -DG method.

Now, the difference of the two discrete Helmholtz–Hodge projectors  $\mathbb{P}_h^{\text{div}}(\mathbf{f}_h) - \mathbb{P}_h^0(\mathbf{f}_h)$  indicates the regions in the flow where a pressure-robust method performs better than a non-pressure-robust one. This is due to the fact that the  $L^2$  Helmholtz projector indicates that the corresponding non-divergence-free method would see a wrong force locally.

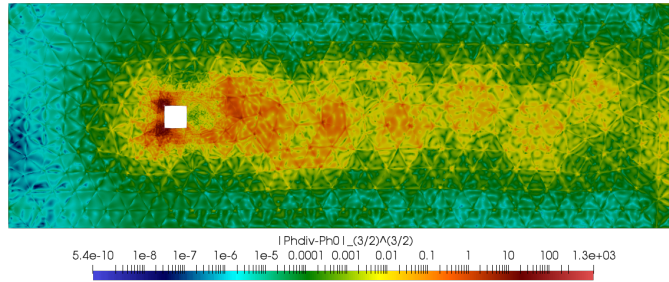


Figure 8: Difference  $|\mathbb{P}_h^{\text{div}}(\mathbf{f}_h) - \mathbb{P}_h^0(\mathbf{f}_h)|_{3/2}^{3/2}$  of the two discrete Helmholtz–Hodge projectors. High values indicate advantageous regions of the pressure-robust discretisation. Note that the colour scale is chosen logarithmically.

Finally, let us demonstrate that by using higher-order, the difference between the discrete Helmholtz–Hodge projectors of the  $L^2$ - and the  $\mathbf{H}(\text{div})$ -DG methods vanishes. Table 1 shows the convergence of the  $L^{3/2}$ -norm of the convective term  $\mathbf{f}_h = (\mathbf{u}_h \cdot \nabla)\mathbf{u}_h$ , the discrete Helmholtz–Hodge projectors  $\mathbb{P}_h^{\text{div}}(\mathbf{f}_h)$  and  $\mathbb{P}_h^0(\mathbf{f}_h)$ , and

their difference  $\mathbb{P}_h^{\text{div}}(\mathbf{f}_h) - \mathbb{P}_h^0(\mathbf{f}_h)$ . One can see that, for example, for  $k = 9$ , both methods detect a comparable amount of divergence-free forces in the discrete convective term. This is a possible explanation why non-pressure-robust methods may work comparably good whenever higher-order methods are considered.

Table 1: Convergence behaviour for  $\mathbf{L}^{3/2}$ -norms of the convective term  $\mathbf{f}_h = (\mathbf{u}_h \cdot \nabla)\mathbf{u}_h$  and its discrete Helmholtz–Hodge projectors for different polynomial orders  $k \in \{2, \dots, 9\}$ .

$k$	2	3	4	5	6	7	8	9
$\ \mathbf{f}_h\ _{\mathbf{L}^{3/2}}$	7.823	8.442	8.239	8.045	7.902	7.85	7.831	7.82
$\ \mathbb{P}_h^{\text{div}}(\mathbf{f}_h)\ _{\mathbf{L}^{3/2}}$	6.884	7.351	7.181	6.935	6.814	6.784	6.774	6.765
$\ \mathbb{P}_h^0(\mathbf{f}_h)\ _{\mathbf{L}^{3/2}}$	7.015	7.381	7.199	6.949	6.824	6.79	6.778	6.767
$\ \mathbb{P}_h^{\text{div}}(\mathbf{f}_h) - \mathbb{P}_h^0(\mathbf{f}_h)\ _{\mathbf{L}^{3/2}}$	1.162	0.502	0.303	0.239	0.198	0.159	0.125	0.098

Consistent with these observation, Figure 9 shows the pointwise plots of the difference between the Helmholtz–Hodge projectors. It is especially interesting that their difference concentrates in the vicinity of the object. This means that pressure-robust methods have a higher accuracy near objects which are located in a flow.

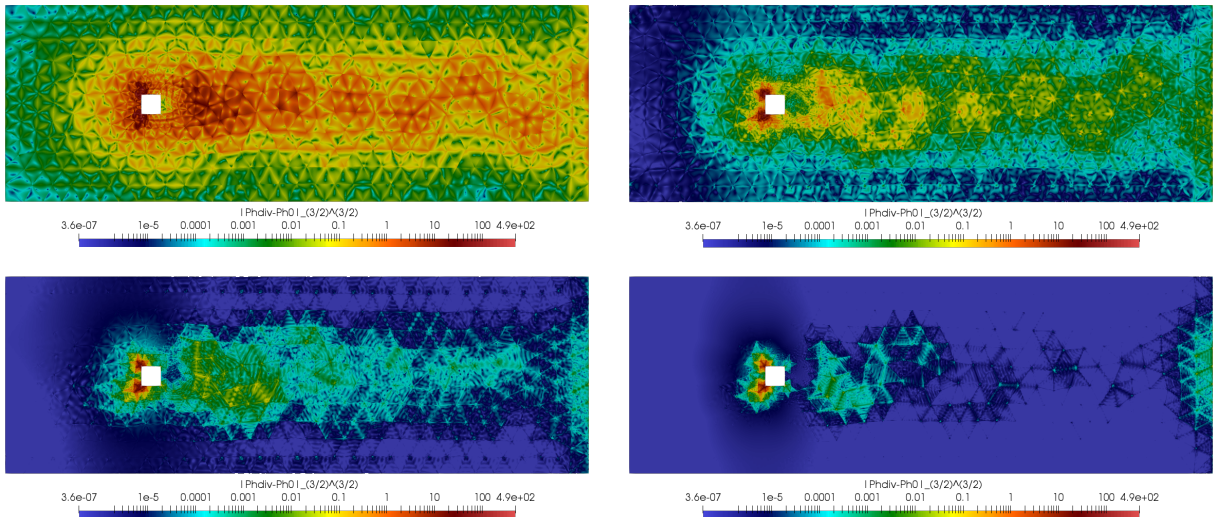


Figure 9: Difference of discrete Helmholtz–Hodge projectors  $\|\mathbb{P}_h^{\text{div}}(\mathbf{f}_h) - \mathbb{P}_h^0(\mathbf{f}_h)\|_{3/2}^{3/2}$  for different polynomial orders  $k \in \{2, 4, 6, 9\}$  (from top left to bottom right).

## 9 Conclusion and outlook

The main intention of this contribution is to show that pressure-robust space discretisations for the incompressible Navier–Stokes equations can dramatically outperform classical space discretisations in certain high Reynolds number flows. Indeed, this is demonstrated for a specific solution set of the incompressible Navier–Stokes equations, the class of generalised Beltrami flows. Since in generalised Beltrami flows the nonlinear convection term is a gradient, generalised Beltrami flows are not only time-dependent Navier–Stokes solutions but also time-dependent Stokes solutions; the only difference is the continuous pressure  $p$ , which is much more complicated in the Navier–Stokes case. Pressure-robust space discretisations are exactly

designed in such a way that they better reflect the Stokes-character of high Reynolds number generalised Beltrami flows on the discrete level.

Last but not least, we now want to give an outlook why we think that better numerical discretisations for generalised Beltrami flows are important for real-world flows and we want go beyond the results achieved in Section 8 on the Kármán vortex street.

1. Actually, as far as we know, all exact Navier–Stokes solutions (i.e., those with right hand side  $\mathbf{f} = \mathbf{0}$ , whose analytical form is known) are of generalised Beltrami type, cf. [20];
2. steady (maybe unstable) high Reynolds number flows with  $\mathbf{f} = \mathbf{0}$ , e.g., around obstacles in the fluid, fulfil (away from boundary layers) the approximate momentum balance

$$(\mathbf{u} \cdot \nabla \mathbf{u}) = -\nabla p + \nu \Delta \mathbf{u} \approx -\nabla p,$$

i.e.,  $(\mathbf{u} \cdot \nabla) \mathbf{u}$  approximates a gradient and  $\mathbf{u}$  approximates a generalised Beltrami flow, thus, cf. [36];

3. such stable and unstable steady high Reynolds number flows were recently shown to play an important role in the transition to turbulence, where the dynamics of certain turbulent flows was described as a *walk between neighbourhoods* of stable and unstable steady flows, cf. [52], i.e., at least *locally in time*, these flows approximate generalised Beltrami flows;
4. the importance of generalised Beltrami flows for turbulence is also backed up by numerical evidence from the 1980s. For example, in [46] numerical experiments for channel flows and homogeneous decaying turbulence indicate that the large-scale turbulent features of a flow behave ‘Beltrami-like’ in regions of low dissipation. In connection therewith, the term ‘local Beltramization’ is, for example, used in [55] and describes the tendency of the flow velocity and vorticity to align locally. In fact, it has even been conjectured that the coherent structures of turbulent flows can be characterised as a superposition of approximate Beltrami flows; see also [17] for a systematic analysis of hierarchies in Beltrami flows;
5. according to the classical Prandtl–Batchelor theorem, the vorticity is constant in those regions of steady 2D flows where viscous forces are small and streamlines are closed. This leads to flows which are of generalised Beltrami type *locally in space*, since the Lamb vector (10) is proportional to the gradient of the (2D) stream function. This result was recently extended to some quasi-periodic 2D flows [4];

Last but not least, we point to recent work where the non-uniqueness of the 3D incompressible Navier–Stokes equations (in the class of weak solutions with finite kinetic energy) is proven. The proof uses certain *intermittent Beltrami flows* which only exist in 3D [13].

All these examples, and more could be given, show that generalised Beltrami flows are not only a very exotic study object but are probably central for the understanding of real world flows. We believe that it is their underlying linear dynamics in the midst of full nonlinearity, which can be recognised by looking at the right equivalence classes of forces (cf. Section 2), which makes them significant. If all this really is true, pressure-robust space discretisation will play an important role in achieving more accurate and efficient numerical simulations in the future.

## References

- [1] N. Ahmed, A. Linke, and C. Merdon. On really locking-free mixed finite element methods for the transient incompressible Stokes equations. *SIAM J. Numer. Anal.*, 56(1):185–209, 2018.
- [2] N. Ahmed, A. Linke, and C. Merdon. Towards pressure-robust mixed methods for the incompressible Navier–Stokes equations. *Comput. Methods Appl. Math.*, 18(3):353–372, 2018.
- [3] M. Akbas, A. Linke, L. G. Rebholz, and P. W. Schroeder. The analogue of grad-div stabilization in DG methods for incompressible flows: Limiting behavior and extension to tensor-product meshes. *Comput. Methods Appl. Mech. Engrg.*, 341:917–938, 2018.

- [4] H. Arbabi and I. Mezic. Prandtl–Batchelor theorem for flows with quasi-periodic time dependence. [arXiv:1808.09398](https://arxiv.org/abs/1808.09398) [physics.flu-dyn], 2018. URL: <https://arxiv.org/abs/1808.09398>.
- [5] D. Arndt, H. Dallmann, and G. Lube. Local projection FEM stabilization for the time-dependent incompressible Navier–Stokes problem. *Numer. Methods Partial Differential Equations*, 31(4):1224–1250, 2015.
- [6] D. N. Arnold, F. Brezzi, and M. Fortin. A stable finite element for the Stokes equations. *Calcolo*, 21(4):337–344 (1985), 1984.
- [7] U. Ascher, S. Ruuth, and B. Wetton. Implicit-explicit methods for time-dependent partial differential equations. *SIAM J. Numer. Anal.*, 32(3):797–823, 1995.
- [8] C. W. Bardos and E. S. Titi. Mathematics and turbulence: where do we stand? *J. Turbul.*, 14(3):42–76, 2013.
- [9] P. B. Bochev, M. D. Gunzburger, and R. B. Lehoucq. On stabilized finite element methods for the Stokes problem in the small time step limit. *Internat. J. Numer. Methods Fluids*, 53(4):573–597, 2007.
- [10] D. Boffi, F. Brezzi, and M. Fortin. *Mixed Finite Element Methods and Applications*. Springer-Verlag Berlin Heidelberg, 2013.
- [11] A. L. Bowers, B. R. Cousins, A. Linke, and L. G. Rebholz. New connections between finite element formulations of the Navier–Stokes equations. *J. Comput. Phys.*, 229(24):9020–9025, 2010.
- [12] F. Boyer and P. Fabrie. *Mathematical Tools for the Study of the Incompressible Navier–Stokes Equations and Related Models*. Springer-Verlag New York, 2013.
- [13] T. Buckmaster and V. Vicol. Nonuniqueness of weak solutions to the Navier–Stokes equation. [arXiv:1709.10033](https://arxiv.org/abs/1709.10033) [math.AP], 2018. URL: <https://arxiv.org/abs/1709.10033>.
- [14] E. Burman and M. A. Fernández. Continuous interior penalty finite element method for the time-dependent Navier–Stokes equations: space discretization and convergence. *Numer. Math.*, 107(1):39–77, 2007.
- [15] M. A. Case, V. J. Ervin, A. Linke, and L. G. Rebholz. A connection between Scott–Vogelius and grad-div stabilized Taylor–Hood FE approximations of the Navier–Stokes equations. *SIAM J. Numer. Anal.*, 49(4):1461–1481, 2011.
- [16] B. Cockburn, G. Kanschat, and D. Schötzau. A note on discontinuous Galerkin divergence-free solutions of the Navier–Stokes equations. *J. Sci. Comput.*, 31(1–2):61–73, 2007.
- [17] P. Constantin and A. Majda. The Beltrami spectrum for incompressible fluid flows. *Commun. Math. Phys.*, 115(3):435–456, 1988.
- [18] D. A. Di Pietro and A. Ern. *Mathematical Aspects of Discontinuous Galerkin Methods*. Springer-Verlag Berlin, 2012.
- [19] O. Dorok, W. Grambow, and L. Tobiska. Aspects of finite element discretizations for solving the Boussinesq approximation of the Navier–Stokes Equations. *Notes on Numerical Fluid Mechanics: Numerical Methods for the Navier–Stokes Equations.*, 47:50–61, 1994.
- [20] P. G. Drazin and N. Riley. *The Navier–Stokes Equations: A Classification of Flows and Exact Solutions*. Cambridge University Press, 2006.
- [21] A. Ern and J.-L. Guermond. *Theory and Practice of Finite Elements*. Springer New York, 2004.
- [22] C. R. Ethier and D. A. Steinman. Exact fully 3D Navier–Stokes solutions for benchmarking. *Int. J. Numer. Meth. Fluids*, 19(5):369–375, 1994.
- [23] M. Fortin and A. Fortin. Newer and newer elements for incompressible flows. *Finite Elements in Fluids*, 6:171–187, 1985.
- [24] L. Franca and T. Hughes. Two classes of mixed finite element methods. *Comput. Methods Appl. Mech. Engrg.*, 69(1):89–129, 1988.
- [25] K. Galvin, A. Linke, L. Rebholz, and N. Wilson. Stabilizing poor mass conservation in incompressible flow problems with large irrotational forcing and application to thermal convection. *Comput. Methods Appl. Mech. Engrg.*, 237/240:166–176, 2012.
- [26] S. Ganesan and V. John. Pressure separation — a technique for improving the velocity error in finite element discretisations of the Navier–Stokes equations. *Appl. Math. Comp.*, 165(2):275–290, 2005.
- [27] J.-F. Gerbeau, C. Le Bris, and M. Bercovier. Spurious velocities in the steady flow of an incompressible fluid subjected to external forces. *Int. J. Numer. Meth. Fluids*, 25(6):679–695, 1997.
- [28] V. Girault, R. H. Nochetto, and L. R. Scott. Max-norm estimates for Stokes and Navier–Stokes approximations in convex polyhedra. *Numer. Math.*, 131(4):771–822, 2015.
- [29] P. M. Gresho, R. L. Lee, S. T. Chan, and J. M. Leone. A new finite element for incompressible or Boussinesq fluids. In *Proceedings of the Third International Conference on Finite Elements in Flow Problems*. Wiley, 1980.
- [30] M. Han Veiga, D. A. Romero Velasco, R. Abgrall, and R. Teyssier. Capturing near-equilibrium solutions: a comparison between high-order discontinuous Galerkin methods and well-balanced schemes. [arXiv:1803.05919](https://arxiv.org/abs/1803.05919) [math.NA], 2018. URL: <https://arxiv.org/abs/1803.05919>.
- [31] K. Hillewaert. Development of the Discontinuous Galerkin Method for High-Resolution, Large Scale CFD and Acoustics in Industrial Geometries. Ph.D. thesis, Université catholique de Louvain, 2013.
- [32] E. Jenkins, V. John, A. Linke, and L. Rebholz. On the parameter choice in grad-div stabilization for the Stokes equations. *Adv. Comput. Math.*, 40(2):491–516, 2014.
- [33] V. John. *Finite Element Methods for Incompressible Flow Problems*. Springer International Publishing, 2016.
- [34] V. John, A. Linke, C. Merdon, M. Neilan, and L. G. Rebholz. On the divergence constraint in mixed finite element methods for incompressible flows. *SIAM Rev.*, 59(3):492–544, 2017.
- [35] G. E. Karniadakis and S. J. Sherwin. *Spectral/hp element methods for CFD*. Numerical Mathematics and Scientific Computation. Oxford University Press, Oxford, second edition, 2013.
- [36] A. Linke. Collision in a cross-shaped domain—a steady 2d Navier–Stokes example demonstrating the importance of mass conservation in CFD. *Comput. Methods Appl. Mech. Engrg.*, 198(41-44):3278–3286, 2009.
- [37] A. Linke. A divergence-free velocity reconstruction for incompressible flows. *C. R. Math. Acad. Sci. Paris*, 350(17-18):837–

840, 2012.

- [38] A. Linke. On the role of the Helmholtz decomposition in mixed methods for incompressible flows and a new variational crime. *Comput. Methods Appl. Mech. Engrg.*, 268:782–800, 2014.
- [39] A. Linke and C. Merdon. Pressure-robustness and discrete Helmholtz projectors in mixed finite element methods for the incompressible Navier–Stokes equations. *Comput. Methods Appl. Mech. Engrg.*, 311:304–326, 2016.
- [40] A. Linke and C. Merdon. Towards pressure-robust mixed methods for the incompressible Navier–Stokes equations. *Comput. Methods Appl. Math.*, 18(3):353–372, 2018.
- [41] A. Linke, C. Merdon, M. Neilan, and F. Neumann. Quasi-optimality of a pressure-robust nonconforming finite element method for the Stokes-Problem. *Math. Comp.*, 87(312):1543–1566, 2018.
- [42] A. Linke and L. G. Rebholz. Pressure-induced locking in mixed methods for time-dependent (Navier–)Stokes equations. [arXiv:1808.07028](https://arxiv.org/abs/1808.07028) [math.NA], 2018. URL: <https://arxiv.org/abs/1808.07028>.
- [43] G. Lube and M. A. Olshanskii. Stable finite-element calculation of incompressible flows using the rotation form of convection. *IMA J. Numer. Anal.*, 22(3):437–461, 2002.
- [44] M. A. Olshanskii, G. Lube, T. Heister, and J. Löwe. Grad-div stabilization and subgrid pressure models for the incompressible Navier–Stokes equations. *Comput. Methods Appl. Mech. Engrg.*, 198(49-52):3975–3988, 2009.
- [45] D. Pelletier, A. Fortin, and R. Camarero. Are FEM solutions of incompressible flows really incompressible? (or how simple flows can cause headaches!). *Internat. J. Numer. Methods Fluids*, 9(1):99–112, 1989.
- [46] R. B. Pelz, V. Yakhot, S. A. Orszag, L. Shtilman, and E. Levich. Velocity-vorticity patterns in turbulent flow. *Phys. Rev. Lett.*, 54:2505–2508, 1985.
- [47] B. Rivière. *Discontinuous Galerkin Methods for Solving Elliptic and Parabolic Equations*. SIAM, 2008.
- [48] F. Schieweck. *Parallele Lösung der Navier–Stokes-Gleichungen*. Habilitation, University of Magdeburg, 1997.
- [49] J. Schöberl. C++11 Implementation of Finite Elements in NGSolve. ASC Report 30/2014, Institute for Analysis and Scientific Computing, Vienna University of Technology, 2014. URL: <https://www.asc.tuwien.ac.at/~schoeberl/wiki/publications/ngs-cpp11.pdf>.
- [50] P. W. Schroeder, C. Lehrenfeld, A. Linke, and G. Lube. Towards computable flows and robust estimates for inf-sup stable FEM applied to the time-dependent incompressible Navier–Stokes equations. *SeMA J.*, 2018. URL: <https://doi.org/10.1007/s40324-018-0157-1>.
- [51] P. W. Schroeder and G. Lube. Pressure-robust analysis of divergence-free and conforming FEM for evolutionary incompressible Navier–Stokes flows. *J. Numer. Math.*, 25(4):249–276, 2017.
- [52] B. Suri, J. Tithof, R. O. Grigoriev, and M. F. Schatz. Unstable equilibria and invariant manifolds in quasi-two-dimensional Kolmogorov-like flow. [arXiv:1808.02088](https://arxiv.org/abs/1808.02088) [physics.flu-dyn], 2018. URL: <https://arxiv.org/abs/1808.02088>.
- [53] R. W. Thatcher and D. Silvester. A locally mass conserving quadratic velocity, linear pressure element, 1987. Numerical Analysis Report No, 147, Manchester University/UMIST.
- [54] H. Xu, C. D. Cantwell, C. Monteserin, C. Eskilsson, A. P. Engsig–Karup, and S. J. Sherwin. Spectral/hp element methods: Recent developments, applications, and perspectives. *J. Hydrodyn.*, 30:1–22, 2018.
- [55] V. Yakhot and S. A. Orszag. Renormalization group and local order in strong turbulence. *Nucl. Phys. B - Proc. Suppl.*, 2:417–440, 1987.
- [56] T. A. Zang. On the rotation and skew-symmetric forms for incompressible flow simulations. *Appl. Numer. Math.*, 7(1):27–40, Jan. 1991.
- [57] S. Zhang. A new family of stable mixed finite elements for the 3D Stokes equations. *Math. Comp.*, 74(250):543–554, 2005.